

# Pyrolysis of spruce wood, wheat straw, switchgrass, miscanthus and swine manure using catalysts containing alkali and alkaline earth metals: thermogravimetric analysis and kinetic modeling

Olivier Fischer<sup>1,2</sup> · Romain Lemaire<sup>1</sup> · Ammar Bensakhria<sup>2</sup>

Received: 28 November 2024 / Accepted: 16 August 2025 © The Author(s) 2025

#### **Abstract**

This paper examines the pyrolysis of 5 biomass types (spruce wood, wheat straw, switchgrass, miscanthus and swine manure) when being catalyzed by additives (NaCl, KCl, CaCl<sub>2</sub> and MgCl<sub>2</sub>) containing alkali and alkaline earth metals (AAEMs). Thermogravimetric analyses (TGA) were carried out with raw samples and with catalyzed ones prepared by wet impregnation. 4 different heating rates (5, 10, 15 and 30 K min<sup>-1</sup>) were used, and the associated experimental data were modeled by implementing 3 isoconversional approaches (Kissinger-Akahira-Sunose (KAS), Flynn-Wall-Ozawa (OFW) and Friedman). The inferred rate constant parameters were then used to compute the variations of the conversion degree of the fuels versus the temperature while considering different reaction mechanisms commonly employed in the literature, including order-based, diffusion, geometrical, nucleation and power law models. As highlights, the results obtained revealed that AAEM catalysts shift the decomposition process to lower temperatures. Besides, conversion profiles computed using each tested modeling approach were found to properly reproduce the TGA results as long as order-based models were selected. An analysis of the kinetic parameters estimated when implementing the three above-listed isoconversional methods showed that the rate constants tend to increase when adding catalysts, with CaCl<sub>2</sub> and MgCl<sub>2</sub> being found to exhibit a stronger capacity to increase pyrolysis rates as compared to NaCl and KCl. Finally, a sensitivity analysis focusing on the impact of the catalyst load on the pyrolysis kinetics revealed a so-called saturation phenomenon indicating that the AAEMs tend to promote the conversion of biomass more effectively when the concentration of metal cation in the impregnating solution is relatively low (not higher than  $\sim 0.15 \text{ mol L}^{-1}$  in the present work).

**Keywords** Biomass · Catalyst · AAEM · TGA · Kinetic analysis

### Introduction

As an energy source, carbon fuels by far lead the pack globally, making renewable alternatives extremely attractive in the devising and implementation of strategies to tackle apparently insatiable energy needs while simultaneously meeting greenhouse gas emission reduction targets. Within this framework, low-emission and carbon-neutral

☐ Romain Lemaire romain.lemaire@etsmtl.ca

Published online: 11 October 2025

- TFT Laboratory, Department of Mechanical Engineering, École de Technologie Supérieure, Montreal, QC H3C 1K3, Canada
- Université de Technologie de Compiègne, ESCOM, TIMR, Centre de Recherche Royallieu - CS 60 319, 60203 Compiègne Cedex, France

renewable energy sources such as biomass are emerging as formidable options as the world seeks to gradually replace conventional fossil fuels. When subjected to pyrolysis under an inert atmosphere, the biopolymers that make up biomass will undergo decomposition, breaking down into biochar, bio-oil and incondensable biogas. The pyrolysis of raw biomass, however, often faces limited conversion yields and selectivity, while pyrolysis products typically exhibit inherent drawbacks attributable to their elevated oxygen content. These drawbacks especially manifest in a low heating value, as well as high corrosiveness and viscosity in the case of bio-oils, which limits their overall usefulness and desirability versus traditional fossil fuels.

To tackle this, a catalytic treatment can be implemented to eliminate undesirable oxygenated groups and produce pyrolysis products having enhanced properties. Various catalysts, such as zeolites, metal oxides and their corresponding



salts, have therefore been explored, and their effects scrutinized, in prior research works (see [1-4], for instance, and references therein). Among currently considered catalysts, particular attention has been devoted to alkali and alkaline earth metals (AAEMs) which are naturally present in biomass and affordable, while exhibiting a low toxicity and a relatively high catalytic efficiency. Various studies have therefore been undertaken during the last decade to elucidate the influences of AAEM catalysts on the nature and distribution of pyrolysis products emitted when thermally treating various biomass types (see [4] and references therein). In their comprehensive review aimed at analyzing the main trends issued from past studies conducted to elucidate the effects of AAEMs on biomass pyrolysis [4], Wang et al. reported that the degradation of biomass was shifted to lower temperatures when the latter was impregnated with AAEM salts while char and gas yields were increased at the expense of bio-oil, whose C/O ratio tends to increase significantly. These observations were, however, shown to depend strongly on the AAEM catalyst considered, as exemplified below.

Conclusions from past studies indeed indicate that adding NaCl to biomass is likely to increase bio-oil yields and decrease the proportions of esters, aldehydes, ketones, organic acids and guaiacols, while promoting the production of anhydrosugars, alcohols and furans. This was notably observed by [5], who showed that the addition of NaCl to rice husk led to the obtention of bio-oils characterized by a lower acidity and a higher heating value. On the other hand, during the pyrolysis of pine wood sawdust catalyzed by sodium hydroxide, sodium carbonate, sodium silicate and sodium chloride, [6] also reported that solid product and gaseous product yields, respectively, increase and decrease. As for potassium, experiments aimed at characterizing the catalytic effect of K<sub>2</sub>CO<sub>3</sub> on the pyrolysis of pine wood showed that this alkali metal allowed to increase char and gaseous product yields (as also noted by [7-9]), while reducing liquid product yields [10]. Potassium was, moreover, shown to suppress the formation of saccharides, aldehydes, alcohols, acids, furans and guaiacols while increasing alkane and phenol yields [10]. Note that this last trend was also reported by [11], who noted an increase in the production of phenol and phenol derivatives during experiments dealing with the pyrolysis of short rotation willow coppice impregnated with potassium acetate. More recently, [12] investigated the thermal degradation characteristics of samples of beech, celluloses, hemicelluloses and lignin impregnated with different concentrations of K<sub>2</sub>CO<sub>3</sub>. The authors then confirmed that potassium addition promotes the decomposition of cellulose and hemicellulose, which shifts the thermal degradation of biomass to lower temperatures, while enhancing the production of char, possibly from the breakage of the glycosidic bonds and the cleaving of hydrogen bonds. A

so-called saturation effect was, moreover, highlighted by the authors, indicating the presence of a limit catalyst concentration above which the effect of potassium is limited. Regarding calcium-based catalysts, they were found to promote biomass pyrolysis, as exemplified by [13], who concluded that calcium chloride significantly lowers the pyrolysis temperature and accelerates the depolymerization of cellulose. According to [4], calcium ions promote biomass degradation through depolymerization, dehydration, decarbonylation, decarboxylation and cracking reactions, thus contributing to reducing the oxygen content of pyrolytic oils [14–17]. This trend was notably observed by Veses et al., who examined the catalytic pyrolysis of forest pine woodchips using calcium-based materials (CaO and CaO·MgO) in an auger reactor [14]. An improvement of the bio-oil properties, including a reduction of both the oxygen content and the acidity, was particularly observed therein, resulting in liquid products exhibiting a higher calorific value and pH. For magnesium catalysts, they were shown to decrease the pyrolysis temperature and the maximum degradation rate of biomass while promoting the formation of volatile compounds with lower molecular weights [8, 18]. Furthermore, they were found to enhance char formation and increase the bio-oil water content, as noted by [19] during experiments conducted on yellow poplar impregnated with MgCl<sub>2</sub>. The formation of oligomers and char fines was especially traced therein to the recombination of levoglucosan and small molecules induced by magnesium, which translated into a higher bio-oil viscosity, molecular weight and solid content [19]. In a recent study focusing on the influence of biomass inorganic components (referred to as BICs) on the pyrolysis characteristics of corncob, [20] concluded that BICs such as K, Na, Ca and Mg accelerate the secondary pyrolysis of corncob and enhance the rearrangement of the char molecular structure, thus increasing the content of molecules such as cyclopentanone and benzenes while decreasing that of furans in the generated products. BICs were finally shown to promote dehydration and keto-enol tautomerism, which resulted in increased C=C, C-H and aromatic structure yields in the char. Finally, observations from past studies globally indicate that alkaline earth metals exhibit a stronger ability to accelerate the decomposition of bulk cellulose and lower its pyrolysis temperature as compared to alkali metals [4]. This was notably demonstrated by [13] in a work dealing with the influence of NaCl, KCl, MgCl<sub>2</sub> and CaCl<sub>2</sub> on cellulose pyrolysis. The authors observed that the mass loss starting temperature was lower when using MgCl<sub>2</sub> instead of CaCl<sub>2</sub>, KCI and NaCl, in order.

Notwithstanding the significant findings reported in the preceding works, very few kinetic analyses have been done on the AAEM-catalyzed pyrolysis of biomass, as highlighted in [4]. Nevertheless, there continues to be a crucial need for properly parameterized kinetic models required for



designing and optimizing pyrolysis reactors. With this in mind, Wang et al. led a series of experimental and modeling efforts aimed at elucidating the effects of various AAEMs on the pyrolysis kinetics of beech wood and corncob [21, 22]. In analyzing the results obtained when impregnating these two feedstocks with Na<sub>2</sub>CO<sub>3</sub>, NaOH, NaCl, KCl, CaCl<sub>2</sub> and MgCl<sub>2</sub>, the authors confirmed that compared to alkaline metals, alkaline earth metals are more effective at fostering biomass decomposition, as can be seen from the greater decreases in characteristic pyrolysis temperatures stemming from the latter [21]. This observation was attributed to the strong affinity of alkaline earth metals for oxygenated groups in biopolymers and to their ability to induce a homolytic fission of glucose rings, the cleavage of glycosidic bonds, dehydration reactions and hemicellulose depolymerization. The mass loss profiles measured by thermogravimetric analyses (TGA) in [21] were then modeled via a Coats-Redfern integral method. The obtained results showed that the pyrolysis rate constants computed at temperatures for which hemicellulose and cellulose decompose increase more significantly when impregnating beech wood and corncob with CaCl<sub>2</sub> and MgCl<sub>2</sub> instead of NaCl and KCl. While the complementary modeling work conducted by [22] using the Ozawa-Flynn-Wall (OFW) and Kissinger-Akahira-Sunose (KAS) isoconversional methods were in keeping with the main trends from the literature reported above, it indicated a reduction of the activation energies of the pyrolysis process when impregnating beech wood with NaCl and KCl, and thus corroborated the presence of catalytic effects shifting the decomposition process to lower temperatures. More recently, [23] investigated the impact of AAEMs on the catalytic pyrolysis of cellulose while focusing on the levoglucosan (LG), bio-oil and biochar yields. The authors notably found that both chloride and acetate salts reduce the LG and biooil yields while increasing that of biochar. Magnesium and calcium chlorides were, moreover, shown to be more effective in decreasing the LG yield than magnesium and chloride acetates, whereas potassium and sodium acetates were conversely found to be more effective than KCl and NaCl. While modeling the TGA results they obtained using the OFW method, [23] finally noted that the activation energy

 $(E_a)$  of cellulose pyrolysis significantly decreases when adding AAEM salts with  $E_a$  values increasing in the following orders:  $(CH_3COO)_2 Mg$ ,  $(CH_3COO)_2Ca < CH_3COOK$ ,  $CH_3COONa$ , KCl,  $NaCl < CaCl_2$ ,  $MgCl_2$ .

Despite the recent findings from [21-23], further research, based on a systematic comparison of the impacts of different AAEMs added to a wide variety of biomass types under the same conditions, is more than ever required, as highlighted in the general review by [4], in order to characterize the catalytic efficiency of each of these additives as a function of the considered feedstock, notably from a kinetic perspective. Given the foregoing, the present work aims at analyzing the pyrolysis kinetics of 5 different feedstocks (spruce wood (SW), wheat straw (WS), swine manure (SM), miscanthus (M) and switchgrass (SG)) impregnated with 4 additives containing AAEMs (NaCl, KCl, CaCl<sub>2</sub> and MgCl<sub>2</sub>). To the best of the authors' knowledge, this is the first time that such a variety of biomass types are considered within a same study dealing with the catalytic effects induced by added AAEM salts, noting that the above works by [21–23] indeed considered no more than two feedstocks. Furthermore, and to better elucidate the so-called saturation phenomenon repsorted by [12] or [21], a sensitivity analysis focusing on the impact of the catalyst load on the pyrolysis kinetics of SW is also proposed herein. For this research, raw and impregnated samples were characterized and pyrolyzed as detailed in Sect. "Experiments and kinetic modeling", which also provides a description of the kinetic models used. The results obtained were then analyzed in Sect. "Results and discussion", where conclusions regarding the influence of the tested AAEM catalysts on the pyrolysis characteristic temperatures, mass loss profiles and pyrolysis kinetics, are drawn.

# **Experiments and kinetic modeling**

## **Feedstocks**

The feedstocks considered herein are spruce wood (SW), wheat straw (WS), swine manure (SM), miscanthus (M)

Table 1 Biochemical analysis and mineral matter content of the biomass samples analyzed in this work

Sample	Biochemic	al analysis/r	nass%—db	Inorgani	Inorganic content/ppm—db								
	Cellulose	Hemicel- lulose	Lignin	Al	Ca	Fe	K	Mg	Na	P	S		
SW	54.5	11.8	26.5	20	898	29	686	161	5	27	44		
WS	37.1	19.0	16.9	40	2997	47	32928	1796	4773	585	1621		
SM	12.4	12.7	6.7	225	24235	8640	15275	5727	3793	10231	8118		
M	51.1	25.8	12.3	100	3644	119	3126	882	101	688	672		
SG	47.6	24.3	11.4	48	3369	82	1685	721	12	440	443		



and switchgrass (SG). Their proximate and ultimate analyses were reported in [24]. As for their biochemical analyses and inorganic contents, also provided in [24], they are displayed again in Table 1 for convenience since the data summarized therein will be especially used to interpret the trends highlighted in Sect. "Results and discussion". Note that, as detailed in [24], the biopolymer contents reported in Table 1 are in keeping with biochemical analyses reported in past studies, and thus, the considered samples are well representative of the investigated biomass types (see [24] and references therein). Note also that during the preparation of the samples, each feedstock was ground and sieved to a smaller than 125 µm size fraction in a bid to limit temperature lags and gradients, which may distort the kinetic parameters ensuing from TGA analyses [25]. Samples were then completely dried for 24 h at 105 °C before being impregnated according to the procedure described in Sect. "Catalysts and impregnation protocol" and/or analyzed as detailed in Sect. "TGA analyses".

# **Catalysts and impregnation protocol**

Four AAEM salts, namely NaCl, KCl, CaCl<sub>2</sub> and MgCl<sub>2</sub>, were selected as catalysts to investigate and compare how monovalent (Na<sup>+</sup> and K<sup>+</sup>) and divalent (Ca<sup>2+</sup> and Mg<sup>2+</sup>) cations influence pyrolysis kinetics. The samples were prepared by wet impregnation, as in [21, 22, 26-32], to foster interactions between the cations and the biomass. The metal chlorides were first mixed with distilled water to obtain solutions having a cation concentration (noted  $C_{\text{cat-i}}$ ) of 0.15 mol  $mL^{-1}$ , which is consistent with the range of values typically considered in [21, 22, 29–31]. 1 g of dried biomass was then dropped into 15 mL of impregnating solution. Following the procedure described in [32], the mixture was stirred for 1 h using a magnetic stirrer, and the impregnated biomass samples were finally vacuum-filtered to remove as much of the impregnating solution as possible before being dried for 24 h at a temperature of 105 °C. Note that for the purposes of the sensitivity analysis of the impact of the catalyst load on the pyrolysis rates, SW samples were also impregnated with the 4 above catalysts while considering solutions having four additional concentrations (0.025, 0.05, 0.3 and 0.5 mol  $L^{-1}$ ).

Although the actual quantity and distribution of added cations in wet-impregnated biomass are seldom detailed (see [26, 32–34] as examples), it is noteworthy that some of the catalyst solution inevitably remains in the biomass after the filtration process, thus forming precipitated crystals after drying. As a consequence, metal cations are typically present in two forms in impregnated samples. They can indeed be bonded to the biomass organic groups or they can be present in the form of precipitated crystals [35]. In order to estimate the total amount of catalyst added to the biomass

while characterizing the distribution of organic and inorganic cations, we used the well-established Mohr titration method [36, 37] to assess the concentrations of chloride ions in both the impregnating solution and the filtrate collected after the impregnation. In short, the concentration of chloride ions in the filtrate (noted  $C_{\text{Cl}^--f}$ ) was calculated using Eq. (1):

$$C_{\text{Cl}^--f} = \frac{FC_{\text{AgNO}_3} V_{\text{eq}}}{V_{\text{f-d}}} \tag{1}$$

where F and  $C_{\rm AgNO_3}$  denote the dilution factor and the concentration of the silver nitrate solution used during the titration process, respectively,  $V_{\rm eq}$  stands for the volume corresponding to the equivalent point for which a silver chromate precipitate is formed in the presence of potassium chromate (1 mL of such a solution being added before the titration as per [37]), while  $V_{\rm f-d}$  is the volume of diluted filtrate. Based on the  $C_{\rm Cl^--f}$  value, one can infer the concentration of Na<sup>+</sup> K<sup>+</sup>, Ca<sup>2+</sup> and Mg<sup>2+</sup> cations in the filtrate (referred to as  $C_{\rm cat-f}$  in the following), noting that one cation is associated with one anion in NaCl and KCl versus two in MgCl<sub>2</sub> and CaCl<sub>2</sub>. The quantity of AAEM cations bonded to the organic groups in biomass (noted  $n_{\rm cat-org}$ ) can then be estimated using Eq. (2):

$$n_{\text{cat-org}} = \frac{\left(C_{\text{cat-i}} - C_{\text{cat-f}}\right)V_{\text{i}}}{m_{\text{b}}} \tag{2}$$

in which  $C_{\mathrm{cat-i}}$  is the concentration of cations in the impregnating solution as stated above,  $V_{\mathrm{i}}$  stands for the volume of impregnating solution and  $m_{\mathrm{b}}$  is the mass of biomass. As far as the quantity of inorganic cations is concerned (referred to as  $n_{\mathrm{cat-inorg}}$  in Eq. (3)), it can be assessed based on the moisture content of the impregnated biomass after filtration (noted MC) following Eq. (3):

$$n_{\text{cat-inorg}} = C_{\text{cat-f}}MC \tag{3}$$

The above quantities (i.e.,  $n_{\rm cat-org}$  and  $n_{\rm cat-inorg}$ ) expressed in mol of cations per mass of biomass can eventually be converted into mass% (denoted  $m_{\rm cat-org}$  and  $m_{\rm cat-inorg}$ ) using the molecular weight of Na, K, Ca and Mg. To conclude, the impregnation rate of cations bonded to organic groups  $(r_{\rm cat-org})$  can be computed as per Eq. (4):

$$b_{\text{cat-org}} = \frac{n_{\text{cat-org}} m_{\text{b}}}{C_{\text{cat-i}} V_{\text{i}}} \tag{4}$$

As can be seen from Table 2, the impregnation rates of organically bonded cations are 16.6 mol% on average for divalent cations versus a mean of 25.0 mol% for monovalent ones. Furthermore, the total mass% of cations impregnated



Table 2 Quantities and distribution of AAEM cations ionically bonded and precipitated as crystals on the surface of SW

Catalyst	$n_{\text{cat-org}}/\text{mol g}^{-1}$	r <sub>cat-org</sub> /mol%	m <sub>cat-org</sub> /mass%	n <sub>cat-inorg</sub> /mol g <sup>-1</sup>	$m_{ m cat-inorg}$ /mass%	m <sub>cat-total</sub> /mass%	organic cations / mass%	inorganic cations / mass%
NaCl	5.6E-04	24.3	1.29	1.8E-04	0.40	1.70	76	24
KCl	5.9E-04	25.7	2.29	1.7E-04	0.66	2.95	78	22
$CaCl_2$	3.7E-04	16.0	1.49	1.9E-04	0.78	2.27	66	34
$\mathrm{MgCl}_2$	4.2E-04	17.2	1.01	2.0E-04	0.49	1.50	68	32

(referred to  $m_{\text{cat-total}}$ ) is below 3 mass%, with a value of 2.95 mass% in the case of potassium, which is perfectly in line with the results reported by [35], who implemented a similar approach for impregnating wood with K<sub>2</sub>CO<sub>3</sub>. The authors indeed estimated that the proportion of potassium in impregnated samples was 3 mass%, with approximately two-thirds of the cations being bonded to the organic fraction, which is globally consistent with the values reported in Table 2. To further validate these results, additional measurements of the inorganic contents of SW samples before and after impregnation with NaCl and MgCl2 were carried out by inductively coupled plasma mass spectrometry (ICP-MS), as was done to obtain the data in Table 1. The total mass% of impregnated cations was then found to be in good agreement with those estimated by the titration method, with a mean relative deviation of less than 10%. Since [35], moreover, showed that the total mass% of cations impregnated was relatively similar (i.e., below 4.5 mass%) for wood, bark or straw with 2/3 of metal bonded to the organic fraction regardless of the considered feedstock, the results summarized in Table 2 thus give good insights into how AAEM cations are added to tested samples during the wet impregnation process. One should, however, note that although metal cations are known to influence the reactivity of surface molecules (see [4] and references therein), a fine characterization of the distribution of the catalysts within the biopolymers would still be a must to better clarify how the interaction between the AAEMs and the impregnated biomass influences the pyrolysis.

# TGA analyses

A thermogravimetric analyzer (SETARAM SETSYS Evolution) was used, similarly to what was done in [38, 39]. The pyrolysis experiments were conducted following the protocol detailed in [24]. A nitrogen flow of 60 mL min<sup>-1</sup> was set and the samples were dried at 378 K for 15 min. The temperature was then upped to 1223 K, with a plateau of 30 min at that temperature. To that end, heating rates of 5, 10, 15 or 30 K min<sup>-1</sup> were used. In all, three repetitions were carried out for each test in order to verify the reproducibility of the data obtained. The kinetic modeling work performed herein was thus conducted based on averaged mass loss profiles.

Of note, the uncertainties reported in Sect. "Results and discussion" were estimated considering a confidence level of 95%, as was the case in [24]. Finally, the conversion degree  $\alpha$  at any given time t (expressed in s) was computed as per Eq. (5) based on  $m_0$  and  $m_\infty$ , which denote the initial and final residual masses assessed for temperatures of 379 and 1223 K:

$$\alpha = 100 \frac{\left(m_0 - m_{\rm t}\right)}{\left(m_0 - m_{\infty}\right)} \tag{5}$$

where  $m_t$  stands for the mass measured at time t.

# **Kinetic modeling**

As mentioned in [24], the evolution of the conversion degree as a function of the temperature T for non-isothermal analysis follows an Arrhenius equation (see Eq. (6)), where k (s<sup>-1</sup>) represents the rate constant, A (s<sup>-1</sup>) denotes the pre-exponential factor,  $E_{\rm a}$  (J mol<sup>-1</sup>) stands for the activation energy, R (8.314 J mol<sup>-1</sup> K<sup>-1</sup>) is the ideal gas constant,  $\beta$  (K s<sup>-1</sup>) corresponds to the heating rate, while  $f(\alpha)$  represents the reaction model:

$$\frac{\mathrm{d}\alpha}{\mathrm{d}t} = k(\mathrm{T})f(\alpha) = A \exp\left(-\frac{E_{\mathrm{a}}}{RT}\right)f(\alpha) \tag{6}$$

The heating rate  $\beta$  during non-isothermal analyses being expressed as  $\beta = dT/dt$ , Eq. (6) can thus be rewritten as follows:

$$\frac{\mathrm{d}\alpha}{\mathrm{d}T} = \frac{A}{\beta} \exp\left(-\frac{E_{\mathrm{a}}}{RT}\right) f(\alpha) \tag{7}$$

In our recent comparison of the capacity of 7 modeling approaches when it comes to simulating the pyrolysis kinetics of the 5 types of biomasses listed in Sect. "Feedstocks", the Friedman, Kissinger–Akahira–Sunose (KAS) and Flynn–Wall–Ozawa (OFW) models were shown to be the most suited [24]. These isoconversional methods,



which are well known for their widespread use in the literature as well as for their ability to accurately capture experimentally monitored results, notably provided the best agreement between measured and simulated conversion degree profiles in [24]. They were therefore considered in the present work to infer the rate constant parameters allowing to account for the pyrolysis of raw and impregnated biomass samples. As for the KAS model, rearranging and integrating Eq. (7), as detailed in [21, 22], leads to the obtention of Eq. (8):

$$\ln\left(\frac{\beta_{i}}{T_{\alpha,i}^{2}}\right) = \ln\left[\frac{A_{\alpha}R}{E_{a,\alpha}g(\alpha)}\right] - \frac{E_{a,\alpha}}{RT_{\alpha,i}}$$
(8)

where the subscripts  $\alpha$  and i, respectively, refer to the given conversion degrees and heating rates while  $g(\alpha)$  denotes the reaction model integral form. Regarding the expression of the OFW model, based on the Doyle's approximation [40], it can be stated as per Eq. (9):

$$\ln \beta_{\rm i} = \ln \left[ \frac{A_{\alpha} E_{\rm a,\alpha}}{Rg(\alpha)} \right] - 5.331 - 1.052 \frac{E_{\rm a,\alpha}}{RT_{\alpha,\rm i}}$$
 (9)

Finally, the equation pertaining to the Friedman method [41] can be expressed as per [42] as follows:

$$\ln \left[ \beta_{i} \left( \frac{d\alpha}{dT} \right)_{\alpha,i} \right] = \ln \left[ A_{\alpha} f(\alpha) \right] - \frac{E_{a,\alpha}}{RT_{\alpha,i}}$$
 (10)

By plotting the evolution of  $\ln(\beta_i/T_{\alpha,i}^2)$ ,  $\ln\beta_i$  and  $\ln\left[\beta_i(\mathrm{d}\alpha/\mathrm{d}T)_{\alpha,i}\right]$  as a function of  $1/T_{\alpha,i}$  for different  $\beta_i$  while taking into account the KAS, OFW and Friedman models, respectively, linearized straight lines are obtained, and their slopes allow to derive  $E_{\mathrm{a},\alpha}$  values, while the intercept allows determining the  $A_\alpha$  values as soon as a proper  $f(\alpha)$  or  $g(\alpha)$  expression is selected.

To identify the best suited reaction models,  $\alpha = f(T)$  graphs were plotted using Eq. (11), which integrated the

activation energies obtained with the above model-free methods.

$$\left(\frac{\mathrm{d}\alpha}{\mathrm{d}T}\right)_{\mathrm{sim}} = \frac{A}{\beta} \exp\left(-\frac{E_{\mathrm{a},\alpha}}{RT}\right) f(\alpha) \tag{11}$$

17 reaction models were tested, including order-based (F1 to F5), diffusion (D2 and D3), geometrical (R2 and R3), nucleation (A2 to A5) and power law (P2 to P5) models. For the calculation, a number  $N_p$ =1550 of theoretical points was selected to compute the conversion degree values on a  $\alpha$  range comprised between 2.5% and 80%. Next, the most suitable reaction model (i.e., that providing the best agreement between measured and simulated conversion degree profiles) was identified. Each tested model's relative ability to properly reproduce experimental data was assessed by computing the root-mean-square deviation (*RMSD*) between theoretical and measured  $\alpha = f(T)$  profiles using Eq. (12):

$$RMSD = \sqrt{\frac{\sum_{T_{\text{exp,l}}=T_{80\%}}^{T_{\text{exp,l}}=T_{80\%}} \left(\alpha_{\text{exp,T}_{\text{exp,l}}} - \alpha_{\text{calc,T}_{\text{exp,l}}}\right)^{2}}{N_{\text{p}}}}$$
(12)

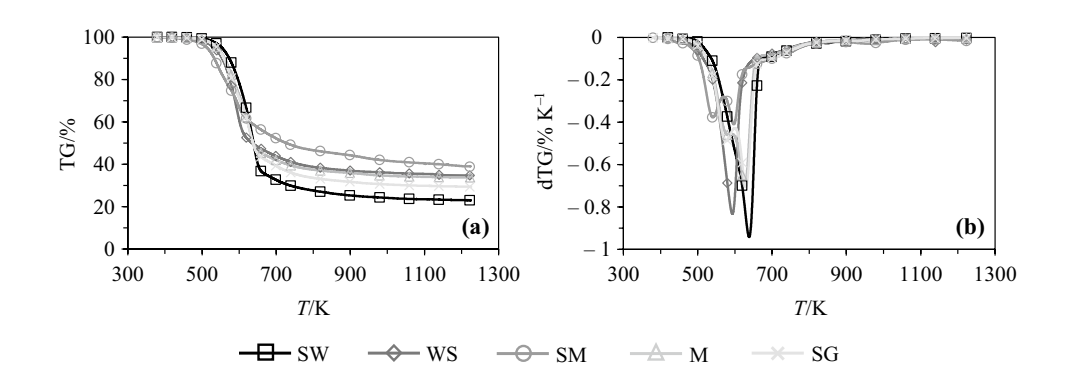
where the subscript l refers to the l <sup>th</sup> point of the series, exp. and calc., respectively, denote experimental and calculated  $\alpha$ , while  $T_{2.5\%}$  and  $T_{80\%}$  stand for the temperatures for which  $\alpha$  reaches values of 2.5% and 80%. The reader is referred to [24] for additional details on the implementation of the kinetic models and the procedure allowing to select a proper reaction model.

# **Results and discussion**

#### **TGA results**

The results issued from the thermogravimetric analyses of the raw feedstocks are plotted in Fig. 1, where the variations of the mass loss (TG) and mass loss rate (dTG) of each sample are reported as a function of the temperature.

Fig. 1 Variation of the mass loss "TG" (a) and derivate mass loss rate "dTG" (b) with the temperature for spruce wood (SW), wheat straw (WS), swine manure (SM), miscanthus (M) and switchgrass (SG) and a heating rate of 10 K min<sup>-1</sup>





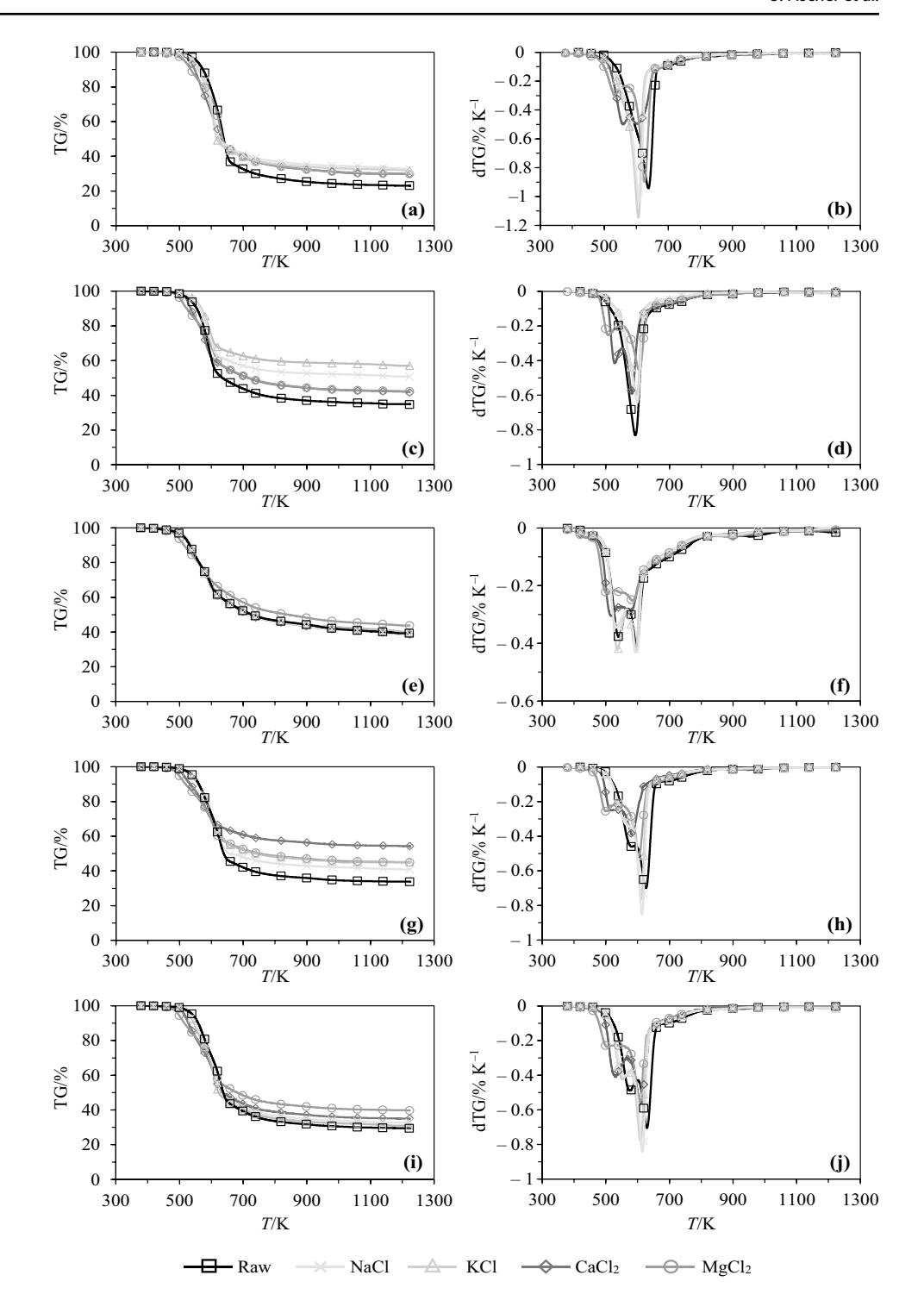
Of note, the TG and dTG curves obtained when pyrolyzing SW, WS, SM, M and SG with heating rates of 5, 10, 15 and 30 K min<sup>-1</sup> were already presented in [24]. As a consequence, only the measurements taken with a  $\beta$  value of 10 K min<sup>-1</sup> are depicted in Fig. 1 as an example, noting that obtained curves exhibit quite similar general features regardless of the heating rate (see [24]). Note also that since the pyrolysis behavior of these different biomass types was commented on in [24], only a short description of the TGA profiles from Fig. 1 will therefore be given herein. In short, one can first note that the decomposition of each sample follows a three-stage process, as commonly observed in the literature [43–48]. This process indeed starts with the removal of water and extractives below 450 K, after which hemicellulose and cellulose rapidly decompose between 450 and 650–700 K. The gently sloping baseline to the dTG curves at high temperatures finally corresponds to the decomposition of lignin, which slowly occurs above 650-700 K. As can be seen from Fig. 1b, the derivate mass loss rate profiles obtained with SW and WS exhibit a single peak, versus two in the case of the other samples, in keeping with the observations previously reported in [48–51]. As detailed in [24], the overlapping peaks observed with SM, M and SG actually produce a single dTG peak with a lower temperature shoulder representing the decomposition of hemicellulose, and a higher temperature peak accounting for the decomposition of cellulose. To better illustrate the main discrepancies existing between the TG and dTG curves depicted in Fig. 1, in Table A1, which is provided in the Appendix for brevity, we summarize the characteristic pyrolysis temperatures, including the temperatures estimated for 10, 50 and 90% conversion degrees (referred to as  $T_{10\%}$ ,  $T_{50\%}$  and  $T_{90\%}$ , respectively) as well as the temperature for which the dTG peaks are recorded (denoted  $T_{\text{max}}$ ). The results obtained then show that the higher the hemicellulose and the lower the cellulose contents in the biomass, the lower the  $T_{\rm max}$ . Furthermore, the higher the sample's inorganic content (as detailed in Table 1), the lower the  $T_{10\%}$  and the higher the residual mass measured at 1223 K (denoted  $TG_{1223K}$  in Table A1). This behavior was especially traced in [24] to the catalytic effect induced by AAEMs (see [24] for more details), thus justifying the interest in a further analysis of the impacts of these metals on biomass pyrolysis, as proposed in the present work.

A comparison between the TGA profiles obtained when analyzing the raw feedstocks and the samples impregnated with NaCl, KCl, CaCl<sub>2</sub> and MgCl<sub>2</sub> is proposed in Fig. 2 for a heating rate of 10 K min<sup>-1</sup>, as an example. For the characteristic pyrolysis temperatures (i.e.,  $T_{10\%}$ ,  $T_{50\%}$  and  $T_{90\%}$ ), the maximum mass loss rate (referred to as  $dTG_{\rm max}$ ) and residual mass at 1223 K obtained from the analysis of the TGA curves, they are detailed in Table A1 for  $\beta$  values of 5, 10, 15 and 30 K min<sup>-1</sup>. The results then clearly show that

impregnating SW, WS, SM, M and SG with sodium, potassium, calcium and magnesium chlorides induces significant changes in the pyrolysis behavior of the studied feedstocks. The plots of Fig. 2 notably show that the AAEM salts tend to shift the decomposition of biomass to lower temperatures, which is particularly exemplified in the case of SW (see Figs. 2a and b), M (see Figs. 2g and h) and SG (see Figs. 2i and j). For a  $\beta$  of 10 K min<sup>-1</sup>,  $T_{10\%}$  indeed decreases by 14.5, 16.5, 26.7 and 41.6 K when adding NaCl, KCl, CaCl<sub>2</sub> and MgCl<sub>2</sub> to SW (see Table A1). A similar trend can, moreover, be observed for the other heating rates. While being in line with the observations by [22] who measured  $T_{10\%}$  decreases of  $\sim$ 11 and  $\sim$ 42 K for  $\beta = 10$  K min<sup>-1</sup> when impregnating beech wood with KCl and MgCl<sub>2</sub>, these results also illustrate the stronger ability of alkaline earth metals to reduce the initial decomposition temperature, as also noted by [9, 52] and further discussed below. The data reported in Table A1 for M and SG further confirm that divalent cations induce higher  $T_{10\%}$  reductions than monovalent ones, with mean decreases (computed based on the four heating rates) of 8.6, 12.0, 54.2 and 42.2 K when adding NaCl, KCl, CaCl<sub>2</sub> and MgCl<sub>2</sub> to M versus values of 10.8, 12.9, 32.6 and 52.7, in the case of SG. In addition, significant reductions of  $T_{\rm max}$ can also be noted when impregnating SW, M and SG with the four above-listed AAEM salts. As examples, the temperature for which the dTG peaks are recorded drops by 26.9 and 38.9 K on average (i.e., considering all the heating rates) when impregnating SW with NaCl and CaCl<sub>2</sub>. Similarly, mean  $T_{\text{max}}$  reductions of 15.0 and 47.4 K occur when impregnating M with sodium and calcium chlorides, versus values of 20.4 and 23.3 K in the case of SG. It is then noteworthy that these observations regarding the effects of AAEMs on the decrease of the pyrolysis temperatures are consistent with the main trends reported in [9, 11, 13, 19, 21, 22, 26–28, 52]. According to these works, and as summarized in [22], the propensity of AAEMs to favor the decomposition of biomass can be traced to their ability to cleave intra- and inter-molecular bonds while favoring the cracking of primary volatiles. Consequently, the yields of light oxygenated compounds and incondensable gaseous species are enhanced [22]. More specifically, sodium cations can act on cellulose through the heterocyclic cleavage of glycosidic linkage and homolytic cleavage in pyranose rings. Further, they interact with the branched-chain structure of hemicellulose to ease rearrangement reactions, depolymerization, dehydration and ring scission [22]. As for potassium, [9] showed that this alkali metal is likely to promote the cleavage of glycosidic bonds and the scission of pyran rings directly by homolytic reaction during the pyrolysis of cellulose. Finally, and as far as calcium and magnesium divalent cations are concerned, they have been demonstrated to enhance hemicellulose degradation while contributing to the initial dehydration/decomposition of cellulose [13,



Fig. 2 Examples of TG ( $\mathbf{a}$ ,  $\mathbf{c}$ ,  $\mathbf{e}$ ,  $\mathbf{g}$ ,  $\mathbf{i}$ ) and dTG ( $\mathbf{b}$ ,  $\mathbf{d}$ ,  $\mathbf{f}$ ,  $\mathbf{h}$ ,  $\mathbf{j}$ ) profiles obtained with a heating rate of 10 K min<sup>-1</sup> for raw and impregnated samples ( $C_{\text{cat-i}} = 0.15 \text{ mol L}^{-1}$ ) of SW ( $\mathbf{a}$ ,  $\mathbf{b}$ ), WS ( $\mathbf{c}$ ,  $\mathbf{d}$ ), SM ( $\mathbf{e}$ ,  $\mathbf{f}$ ), M ( $\mathbf{g}$ ,  $\mathbf{h}$ ) and SG ( $\mathbf{i}$ ,  $\mathbf{j}$ )



19, 53, 54] through various mechanisms (e.g., dehydration, depolymerization, etc.), which were reviewed in [4]. That alkaline earth metals are more efficient at reducing the initial pyrolysis temperatures than alkali metals, as observed herein, can be traced to the strong affinity of alkaline earth metals to biopolymer oxygenated groups and to their ability to foster hemicellulose and cellulose depolymerization [27, 55, 56]. Indeed, and as mentioned above, divalent cations

(e.g.,  $\mathrm{Mg^{2+}}$ ) are particularly prone to promote the pyrolysis of hemicellulose and the initial decomposition of cellulose [19, 54]. On the other hand, monovalent cations (e.g.,  $\mathrm{K^{+}}$  and  $\mathrm{Na^{+}}$ ) notably promote the conversion of levoglucosan, which is typically issued from the pyrolysis of cellulose [8]. This thus explains why higher reductions of  $T_{10\%}$  are experimentally assessed when alkaline earth metals are used instead of alkali ones (as noted by [13, 27, 54]), the former



being indeed more prone to act on hemicellulose, which decomposes at a lower temperature than cellulose.

The profiles of Fig. 2 indicate that alkaline earth metals also tend to change the shape of the mass loss and mass loss rate curves in the case of SW and WS. Indeed, while the dTG curves recorded for raw SW and SW impregnated with NaCl and KCl are characterized by a single peak when the temperature reaches values around ~639, ~611 and ~607 K, respectively, the peaks of the dTG curves relating to SW impregnated with MgCl<sub>2</sub> and CaCl<sub>2</sub> are observed for temperatures of ~626 K and ~602 K, respectively, with distinct shoulder peaks located on the left for temperatures ~43 K (CaCl<sub>2</sub>) and ~92 K (MgCl<sub>2</sub>) lower. Similarly, and unlike the dTG curves recorded for raw WS and WS impregnated with NaCl and KCl, which comprise single peaks at ~592, ~599 and ~597 K, respectively, the dTG curves obtained for WS impregnated with CaCl<sub>2</sub> and MgCl<sub>2</sub> are characterized by main peaks for temperatures of ~582 K and ~604 K, respectively, with shoulder peaks located at ~54 K (for CaCl<sub>2</sub>) and ~96 K (for MgCl<sub>2</sub>) below the temperature corresponding to the maximum mass loss rate (see Fig. 2). The formation of similar shoulder peaks was actually also observed by [23] during TGA experiments conducted with cellulose impregnated with CaCl<sub>2</sub> and MgCl<sub>2</sub>. According to [9], this phenomenon would be related to the cleavage of the glycosidic bonds by the retro-Diels-Alder reaction after cellulose dehydration. Finally, and contrary to what was reported above for SW, M and SG, adding KCl and NaCl to WS and SM appears to have no significant effect on the measured characteristic pyrolysis temperatures (see Fig. 2 and Table A1). Slight increases of  $T_{10\%}$  and  $T_{max}$  are even measured in these cases. For instance, the mean  $T_{10\%}$ computed considering all the heating rates rise by 0.6 and 2.3 K when impregnating SM with NaCl and KCl. The corresponding values in the case of WS are 6.5 and 4.4 K, while for their part, the increase of the mean  $T_{\text{max}}$  values is 8.0 and 5.9 K. That said, this specific behavior could potentially be induced by the high amount of sodium and potassium contained in these feedstocks (see Table 1). Indeed, and as evidenced by [12, 21], a so-called saturation phenomenon is likely to make WS and SM less sensitive to further NaCl and KCl addition, a point further addressed in Sect. "Influence of the catalyst load".

To conclude, Fig. 2a, c, e, g and l, as well as Table A1, illustrates that the  $TG_{1223\,\mathrm{K}}$  values increase when impregnating the tested feedstocks with NaCl, KCl, CaCl<sub>2</sub> and MgCl<sub>2</sub>. For a heating rate of 10 K min<sup>-1</sup> as an example, the residual mass at 1223 K goes from 22.5% for raw SW to 32.4%, 31.7%, 29.9% and 29.8% when considering the samples impregnated with NaCl, KCl, CaCl<sub>2</sub> and MgCl<sub>2</sub>, respectively. Here as well, this trend, which is in line with the observations from [8, 11, 19, 32, 52, 56, 57], may have to do with an enhanced formation of char and/or recombination

reactions occurring at the final pyrolysis stage. AAEMs can indeed promote recombination reactions culminating in char production thanks to their role as bridges that link adjacent oxygenated functional groups [4]. Particularly, NaCl can reduce the yields of levoglucosan from cellulose as a result of the polymerization of volatile levoglucosan, which can enhance char formation [8, 18]. As for magnesium chloride, it can promote repolymerization reactions and thus contribute to increasing char production [13]. According to [56], magnesium ions can catalyze secondary pyrolysis reactions and hence convert anhydrosugar into secondary char. Mg<sup>2+</sup> is, moreover, believed to catalyze reactions between volatile molecules to promote recombination reactions leading to the formation of char [19]. It is still noteworthy that the increases of the residual masses measured with SW and WS are higher when alkali metals (Na and K) are used as catalysts instead of alkaline earth metals (Ca and Mg). While agreeing with the observations made in [22], where the pyrolysis of raw beech wood was compared with that of samples impregnated with NaCl, KCl and MgCl<sub>2</sub>, this observation is also in line with the conclusions drawn by [58], who reported that although both alkali and alkaline earth metals increase the yield of char during the fast pyrolysis of lignin, the char promoting effect of alkali metals was still found to be much greater. Diverging results can, however, be noted in the case of SM, M and SG, which exhibit widely varying biochemical compositions with higher hemicellulose and lower lignin contents (see Table 1). For instance, the residual masses measured with SG having hemicellulose and lignin contents of 24.3 and 11.4 mass%, respectively, are higher when using CaCl2 and MgCl2 as catalysts instead of NaCl and KCl, which is opposite to what was found with SW, whose hemicellulose and lignin contents are 11.8 and 26.5 mass% (see Table 1). These contradictory trends, however, agree with the observations made in [21], where higher residual masses were measured when impregnating corncob with alkaline earth metals instead of alkali ones, although the opposite was noted when using beech wood instead, which comprises less hemicellulose and more lignin [21, 22]. Although many factors (e.g., biochemical composition and amount of inherent AAEMs in the samples, presence of lipids or proteins in the biomass, as is the case for SM, for instance [24], etc.) have to be considered when it comes to thoroughly interpreting such pyrolysis behavior discrepancies, the above results still tend to show that the char promoting effect of calcium- and magnesium-containing catalysts is likely to be smaller than that of sodium and potassium ones when the hemicellulose content of the biomass is low. This would actually be consistent with the action of alkaline earth metals which influence the hemicellulose decomposition in a selective manner [19, 21, 54]. This has been especially exemplified herein by the fact that the highest reductions of  $T_{10\%}$  measured when alkaline earth metals are selected as



catalysts are obtained with M and SG, which are the samples containing the highest amounts of hemicellulose (see [4] and references therein for more information on the way AAEMs specifically influence the mechanisms involved in the decomposition of the main biomass components). All these observations thus illustrate that the results we obtained are consistent, although the modeling work proposed in Sect. "Impact of AAEMs on pyrolysis kinetics" will help to further interpret the highlighted trends, while providing insights into how the different AAEMs affect the pyrolysis kinetics.

# Impact of AAEMs on pyrolysis kinetics

# Assessment of rate constant parameters

The isoconversional method implementation detailed in Sect. "Kinetic modeling" led to the obtention of the activation energies reported in Table 3 for WS, SM and SG, as examples (the values of the pre-exponential factors being, for their part, commented on further below in this section). Although we computed the  $E_a$  values for each 5% step of the conversion degree, only the activation energies corresponding to  $\alpha$  of 20, 50 and 80% are reported therein, for brevity. Furthermore, the procedure allowing to infer rate constant parameters by means of the KAS, OFW and Friedman models, as well as the values of the rate constant parameters estimated for the raw biomass samples, has already been presented and discussed in [24]. Only a few examples of results will therefore be provided below, with the focus being more specifically on the analysis of the effects of AAEMs on pyrolysis rates.

The data listed in Table 3 show that the activation energies derived from the implementation of the KAS and OFW models are quite similar. The mean difference between the  $E_{\rm a}$  estimated with both these modeling approaches while considering each feedstock (i.e., SW, WS, SM, M and SG), each catalyst (i.e., NaCl, KCl, CaCl2 and MgCl2) and the entire range of conversion degrees (i.e.,  $5\% \le \alpha \le 90\%$ ) is only  $\sim 3.5\%$ , which agrees with what was previously found in [24] (i.e.,  $\sim$ 4%). Alternatively, and as was observed in [24], a higher discrepancy can be noted when comparing the  $E_a$ estimated using the KAS and OFW models with those issued from calculations performed with the Friedman method. The mean relative deviation between the activation energies inferred using the Friedman and OFW models is 8.4% (versus 7.4% in [24]), while it is 11.2% (versus 11.6% in [24]) when comparing the Friedman and OFW methods. One can further note that the  $E_a$  reported in Table 3 increases with the conversion degree, which is in keeping with the fact that more energy is required to release the species emitted at high temperatures. It is noteworthy that the addition of NaCl and KCl to WS induces significant decreases of the activation energies regardless of the considered model. The mean  $E_a$  values computed for  $5\% \le \alpha \le 90\%$  indeed drop by ~14.2 (NaCl) and ~12.1 (KCl) kJ mol<sup>-1</sup> when considering the KAS model versus values of ~13.4 and ~11.4 kJ mol<sup>-1</sup> for the OFW method and ~17.4 and ~16.1 kJ mol<sup>-1</sup> with the Friedman model. Of note, similar trends are also observed with SW, with reductions of the mean activation energies up to 12.3 kJ mol-1 when considering KCl as a catalyst and the KAS model (corresponding values being 12.0 and 13.2 kJ mol-1 with the OFW and Friedman methods, respectively). The activation energy representing the minimum energy required for a reaction to occur;  $E_a$  reductions thus suggest that the amount of energy required to overcome the energy barrier allowing pyrolysis to occur is smaller. While these observations are in line with the order of magnitude of the  $E_a$  decreases previously noted by [22], they also tend to confirm the observations in Sect. "TGA Results" regarding the enhanced biomass decomposition induced by alkali metals. As can be seen by looking at the results obtained with SM and SG, a smaller reduction of the activation energies can also be observed when adding KCl to these feedstocks (-10.1 kJ mol<sup>-1</sup> and -2.3 kJ mol<sup>-1</sup> on average when considering the Friedman model). On the other hand, impregnating SM and SG with NaCl induces marginal reductions, and even increases of the activation energies, as is also the case when using CaCl<sub>2</sub> and MgCl<sub>2</sub>, regardless of the biomass considered. Actually, the fact that magnesium induces limited reductions and even increases of  $E_a$  was also observed in [22]. One should, however, note that properly assessing the ability of AAEMs to promote pyrolysis reactions requires computing the rate constants k which integrate the activation energies as well as the pre-exponential factors (see Eq. (6)) whose values can be inferred once proper  $f(\alpha)$ or  $g(\alpha)$  formulations are selected. 17 reaction models (see Sect. "Kinetic modeling") were thus tested in order to identify those leading to the best agreement between simulated and experimentally derived conversion degree profiles (see [24] for more details regarding this procedure). Based on the mean RMSD computed for each biomass (considering both raw and impregnated samples), the following reaction models were identified as being the best suited: F1 for SW and WS, F5 for SM and F2 for M and SG when the KAS and Friedman methods are used, versus F3 for SW and WS, F5 for SM and F4 for M and SG when implementing the OFW method. Regardless of whether or not the samples were impregnated with AAEMs, order-based models were systematically identified as being the most appropriate. Some discrepancies were, however, sometimes observed, depending on the considered feedstock and catalyst. As an example, while F1 was identified as being best suited with the KAS model for raw WS and samples impregnated with NaCl and KCl, F3 was alternatively found to perform slightly better in reproducing the evolution of  $\alpha$  as a function of T when CaCl<sub>2</sub> was considered as a catalyst. Similarly, the RMSD



**Table 3**  $E_{a,\alpha}$  and  $A_{\alpha}$  values assessed for 20, 50 and 80% conversion degrees, as examples, using the KAS, OFW and Friedman modeling approaches for raw and impregnated WS, SM and SG samples

Kinetic parameters			Ea,α	$A_{\alpha}$	Ea,α	$A_{\alpha}$	Ea,α	Αα	Ea,α	Aα	Ea,α	Aα
			/kJ mol <sup>-1</sup>	/s <sup>-1</sup>	/kJ mol <sup>-1</sup>	/s <sup>-1</sup>	/kJ mol <sup>-1</sup>		/kJ mol <sup>-1</sup>	/s <sup>-1</sup>	/kJ mol <sup>-1</sup>	/s <sup>-1</sup>
Sample	Model	$\alpha$ /%	Raw		NaCl		KCl		CaCl <sub>2</sub>		$MgCl_2$	
WS	KAS	20	92.6	5.2E+05	86.7	1.2E+05	88.3	1.7E+05	104.1	1.8E+07	118.5	9.2E+08
		50	107.2	1.2E+07	98.3	1.5E+06	100.6	2.6E+06	147.7	1.0E+11	157.9	4.8E+11
		80	164.2	1.4E+11	132.7	4.4E+08	135.4	5.0E+08	161.9	3.6E+10	148.2	3.8E+09
	OFW	20	97.1	2.5E+06	91.5	6.4E+05	93.0	9.2E+05	107.6	6.4E+07	121.1	2.4E+09
		50	111.4	8.4E+07	103.0	1.3E+07	105.2	2.1E+07	149.7	3.6E+11	159.6	1.6E+12
		80	166.6	1.7E+12	136.6	8.3E+09	139.3	9.3E+09	164.7	4.9E+11	151.5	6.1E+10
	Friedman	20	108.3	1.6E+07	100.4	2.7E+06	103.6	5.3E+06	125.9	2.0E+09	139.7	5.3E+10
		50	117.7	1.0E+08	106.0	8.8E+06	108.5	1.5E+07	161.8	1.1E+12	155.1	1.1E+11
		80	177.0	1.5E+11	145.4	5.6E+08	144.9	3.3E+08	184.1	1.9E+11	162.9	6.6E+09
SM	KAS	20	94.4	3.0E+06	96.6	5.1E+06	95.8	4.5E+06	103.5	4.7E+07	107.1	1.5E+08
		50	109.2	8.1E+07	104.4	2.9E+07	100.4	1.5E+07	117.7	6.1E+08	115.0	2.9E+08
		80	171.8	2.1E+12	186.4	1.8E+13	158.8	2.6E+11	186.1	2.3E+13	161.9	2.1E+11
	OFW	20	98.3	1.0E+07	100.5	1.7E+07	99.7	1.5E+07	106.8	1.3E+08	110.2	3.6E+08
		50	113.4	2.5E+08	108.9	9.8E+07	105.0	5.4E+07	121.4	1.6E+09	118.8	8.2E+08
		80	175.0	3.9E+12	188.9	2.9E+13	162.6	5.7E+11	188.5	3.8E+13	165.7	4.6E+11
	Friedman	20	104.9	4.1E+07	107.3	6.3E+07	104.4	4.5E+07	113.1	4.0E+08	111.0	2.5E+08
		50	116.6	5.7E+08	111.0	1.8E+08	106.0	8.2E+07	123.7	2.0E+09	112.4	1.6E+08
		80	189.3	2.2E+13	202.4	1.3E+14	171.0	1.2E+12	204.8	3.1E+14	158.5	7.2E+10
SG	KAS	20	85.1	8.1E+04	96.9	2.9E+07	90.0	4.0E+05	105.0	2.9E+07	119.6	1.7E+09
		50	105.3	4.6E+06	112.5	3.3E+08	107.5	1.2E+07	122.0	3.3E+08	122.4	3.8E+08
		80	123.5	1.4E+08	134.8	3.1E+08	125.3	1.2E+08	126.5	3.1E+08	146.7	8.8E+09
	OFW	20	90.1	4.7E+05	101.1	1.0E+08	94.5	2.0E+06	108.4	1.0E+08	122.0	4.4E+09
		50	109.9	3.8E+07	116.7	2.0E+09	111.8	9.0E+07	125.5	2.0E+09	125.8	2.2E+09
		80	127.8	4.1E+09	138.9	8.9E+09	129.8	3.7E+09	130.7	8.9E+09	150.1	2.0E+11
	Friedman	20	96.8	1.3E+06	112.5	3.8E+08	103.7	8.5E+06	117.1	3.8E+08	117.8	5.4E+08
		50	116.4	3.7E+07	116.1	2.4E+09	112.3	3.5E+07	133.8	2.4E+09	126.2	5.7E+08
		80	126.5	7.8E+07	146.2	1.2E+07	137.3	2.7E+08	114.5	1.2E+07	136.9	4.6E+08

estimated when using the F5 model instead of the F4 one to simulate the conversion degrees of SG impregnated with MgCl<sub>2</sub>, while considering the OFW modeling approach, was 3.2% instead of 3.9%. These RMSD variations (less than 1%) are quite marginal, however, especially when considering the uncertainties encompassing the measurements and modeling procedures (see [24], where a discussion on the matter is proposed). This is the reason why, for simplicity, the  $f(\alpha)$  and  $g(\alpha)$  formulations were selected based on mean RMSD values computed for each biomass type, as stated above. This notably explains why the F5 and F2 models were selected for SM and M with the KAS method herein, versus the F4 and F1 models in [24], where the RMSD were computed solely based on data obtained with raw feedstocks.

Integrating the activation energies and pre-exponential factors listed in Table 3 in the expression of the rate constant (see Eq. (6)) led to the obtention of the k = f(T) graphs plotted in Fig. 3. Note that only the results obtained with the commonly used KAS model and a heating rate of  $10 \text{ K min}^{-1}$  are depicted in this figure for brevity (similar trends being obtained when considering the OFW and Friedman modeling approaches and the other tested heating rates).

As for the results obtained with SW, WS, M and SG, they show that CaCl2 and MgCl2 significantly enhance the rate constants at low temperatures (from ~500 to ~600 K), which is typical of the onset of the pyrolysis process characterized by the decomposition of hemicellulose and the initial dehydration/decomposition of cellulose. This observation is, moreover, perfectly in line with the  $T_{10\%}$  reductions highlighted in Sect. "TGA Results". Alternatively, and in agreement with the characteristic temperatures reported in Table A1, the enhancement of k is much weaker with SM. This trend can notably be traced to the relatively low hemicellulose and cellulose contents of SM (see Table 1), reiterating that alkaline earth metals more particularly influence the decomposition of these specific biopolymers in a selective fashion. Furthermore, the high amount of inherent Ca and Mg contained in this biomass (see Table 1) is likely to make it less sensitive to further calcium and magnesium addition due to the so-called saturation phenomenon, which will be further examined in Sect. "Influence of the catalyst load". Regarding potassium and sodium-based catalysts, their effects on k are much weaker, as evidenced by the curves corresponding to SW, M and SG in Fig. 3. Similar



and even slightly lower k values can even be observed when impregnating WS and SM with KCl and NaCl, which is consistent with the values of the characteristic pyrolysis temperatures commented on in Sect. "TGA results". Here again, this observation may be related to the high inherent K and Na contents in these feedstocks (see Table 1), thus making it less likely for them to be influenced by the addition of potassium and calcium chlorides through wet impregnation. Actually, the greater ability of alkaline earth metals to influence the pyrolysis kinetics as compared to alkali metals is in keeping with the fact that the former are more prone to weaken the strength of the intramolecular bonds of biopolymers, thereby facilitating the low-temperature decomposition of biomass [19]. This is, moreover, consistent with the conclusions by [59], who showed that, unlike magnesium and calcium, sodium and potassium ions do not significantly influence the activation barriers of glycosidic bond cleavage reactions. Finally, it is noteworthy that, regardless of the selected catalyst, the enhancement of k tends to vanish at relatively high temperatures (i.e., ~655 K for SW, M, SG, ~620 K for WS and ~590 K for SM), which, here again, is consistent with the fact that AAEMs mainly favor the decomposition of hemicellulose and cellulose, which occurs for temperatures below ~650 K [4].

# Comparison of simulated and measured conversion degree profiles

In Fig. 4, we plot the conversion degree profiles corresponding to WS, SM and SG samples impregnated with KCl and CaCl<sub>2</sub> for a 10 K min<sup>-1</sup> heating rate. Measured data are especially compared therein with simulated ones derived from the implementation of the KAS, OFW and Friedman models while integrating the reaction mechanisms previously identified as being the best suited in Sect. "Assessment of rate constant parameters". Note that for clarity, only the results obtained with one alkali and one alkaline earth metal are plotted in Fig. 4. We indeed previously showed that Na and K, as well as Ca and Mg, tend to similarly influence the pyrolysis process. Furthermore, only 3 biomass types and one heating rate were selected to plot the graphs of Fig. 4, for brevity, noting that a similar agreement between predicted data and experimental ones can be observed when considering the pyrolysis tests conducted using the other

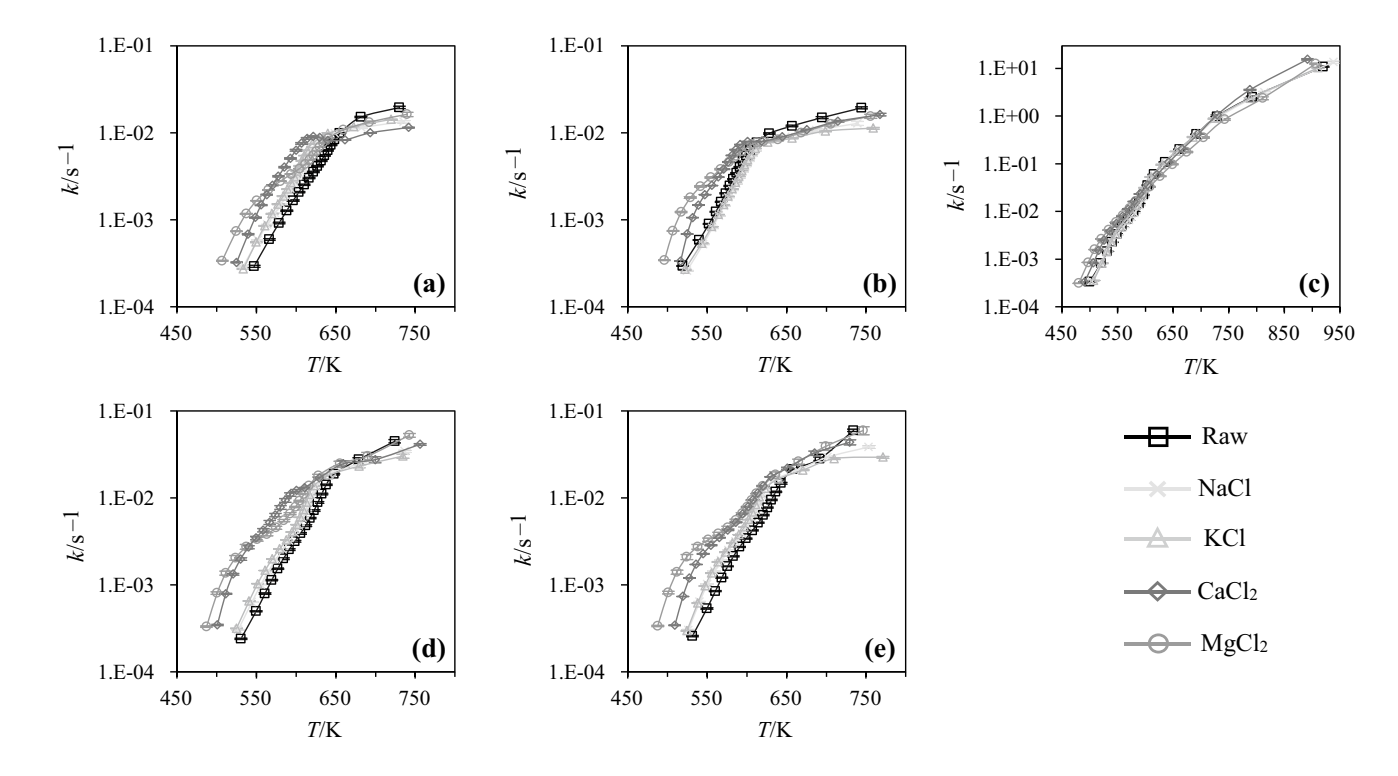


Fig. 3 Evolution of the rate constant values estimated by means of the KAS model as a function of the temperature for raw and catalyzed SW (a), WS (b), SM (c), M (d) and SG (e) samples for a heating rate of 10 K min<sup>-1</sup>



feedstocks and heating rates. For more details, the reader is referred to [24], where a comparison between simulated and measured  $\alpha = f(T)$  plots is proposed for raw SW, WS, SM, M and SG samples when using 7 different kinetic models, including the KAS, OFW and Friedman ones. In addition, conversion profiles for SW impregnated with NaCl and MgCl<sub>2</sub> can also be found in [60], where curves simulated using the KAS, OFW and Friedman methods were compared with experimental data.

The obtained curves illustrate that the KAS and OFW models satisfactorily reproduce measured data regardless of the considered catalyst (similar results being obtained for raw biomass samples as stated above and exemplified in [24]). The predictions of the Friedman model, however, better match measured data, which is noticeable for the WS and SG samples impregnated with CaCl<sub>2</sub>, for instance. This is especially corroborated by the mean RMSD values (averaged based on the 4  $\beta$  used, the 5 biomass types, the 4 catalysts and each conversion degree between 5 and 90%): ~1.0% for the Friedman modeling approach versus ~3.5% on average for the KAS and OFW methods. This thus confirms the observations in [24] regarding the predictive capability of the models tested in this work, which follows the Friedman > KAS ≈ OFW order. That being said, and despite the slightly better agreement obtained when implementing the Friedman model, each considered isoconversional model qualitatively and quantitatively captures the experimental profiles, regardless of the  $\alpha$  values. This thus tends to illustrate the consistency of the parameters derived in Sect. "Assessment of rate constant parameters" while also corroborating the relevance of the analyses conducted therein regarding the impact of AAEMs on pyrolysis kinetics. The validity of the parameterized models used in this work being demonstrated, these simulation tools were therefore used to investigate the so-called saturation phenomenon, which

has seldom been analyzed from a kinetic perspective in the literature, as evidenced in Sect. "Introduction".

### Influence of the catalyst load

In order to investigate the impact of the catalyst load on the pyrolysis kinetics, SW samples were impregnated with catalyst solutions containing different concentrations of NaCl, KCl, CaCl<sub>2</sub> and MgCl<sub>2</sub> (i.e., 0.025, 0.05, 0.15, 0.3 and 0.5 mol L<sup>-1</sup>). Of note, SW was selected for this sensitivity analysis as its inherent sodium, potassium, calcium and magnesium contents are quite low as compared to the other considered feedstocks (see Table 1), which will thus help isolate the influence of added AAEMs. The TGA curves depicting the evolution of the mass loss and mass loss rate of each sample as a function of the temperature are presented in Fig. 5 for a  $\beta$  value of 5 K min<sup>-1</sup> as an example. As for the characteristic decomposition temperatures ( $T_{10\%}$  and  $T_{\rm max}$ ), maximum mass loss rate ( $dTG_{\rm max}$ ) and residual mass at 1223 K  $(TG_{1223 \text{ K}})$  derived from the TGA curves obtained for  $\beta = 5 \text{ K min}^{-1}$ , they are summarized in Table 4.

The curves plotted in Fig. 5 and the characteristic temperatures reported in Table 4 firstly show that the shift of the biomass decomposition to lower temperatures is enhanced by the concentration of the catalyst in the impregnating solution. This is notably exemplified by the fact that the higher the  $C_{\rm cat-i}$  value, the lower the  $T_{10\%}$  and  $T_{\rm max}$  values, regardless of the considered AAEM. The  $T_{10\%}$  values indeed decrease from 549.5 K for raw SW to 538.4, 535.8, 527.7 and 514.0 K when this biomass is impregnated with NaCl, KCl, CaCl<sub>2</sub> and MgCl<sub>2</sub>, respectively, while considering a  $C_{\rm cat-i}$  of 0.15 mol L<sup>-1</sup> (corresponding values being 534.3, 530.3, 526.0 and 505.6 K for  $C_{\rm cat-i} = 0.5$  mol L<sup>-1</sup>). Likewise,  $T_{\rm max}$  drops from 622.8 K for raw SW to 594.8, 590.3, 605.5 and 612.7 K in the case of the samples impregnated with solutions of NaCl, KCl, CaCl<sub>2</sub> and MgCl<sub>2</sub> having a

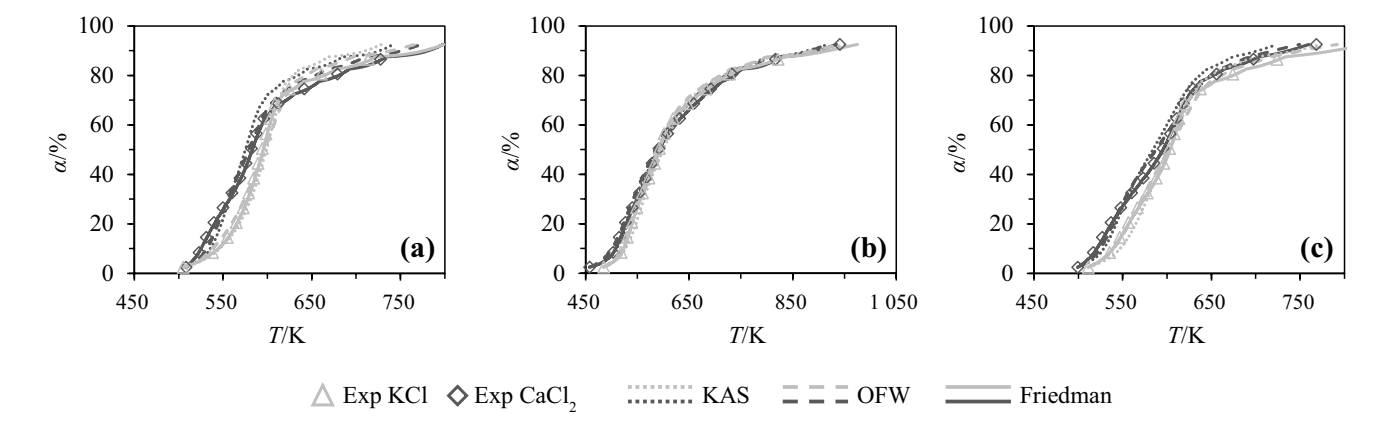


Fig. 4 Comparison of measured and simulated conversion profiles obtained with WS (a), SM (b) and SG (c) impregnated with KCl (light gray) and  $CaCl_2$  (dark gray) for a heating rate of  $10 \text{ K min}^{-1}$ 



concentration of cations of 0.15 mol L<sup>-1</sup> (corresponding values being 592.4, 588.4, 579.7 and 605.7 K for  $C_{\text{cat-i}} = 0.5 \text{ mol L}^{-1}$ ). Regarding alkaline earth metals, it is noteworthy that a minimum  $C_{\text{cat-i}}$  of 0.15 mol L<sup>-1</sup> is required when impregnating SW with CaCl<sub>2</sub> and MgCl<sub>2</sub> to observe the formation of a shoulder peak located on the left of the mean peak for temperatures ~39 K (CaCl<sub>2</sub>) and ~83 K (MgCl<sub>2</sub>) lower on average. Besides, the data reported in Table 4 for CaCl<sub>2</sub> and MgCl<sub>2</sub> also show that  $T_{10\%}$  decreases much more when  $C_{\text{cat-i}}$  increases from 0.05 and 0.15 mol L<sup>-1</sup> than when it is raised from 0 to 0.05 mol L<sup>-1</sup> (–15.9 K versus –5.9 K for CaCl<sub>2</sub> and –27.9 K versus –7.6 K for MgCl<sub>2</sub>). This observation thus tends to indicate that a minimum concentration of catalyst is required to weaken the chemical bonds within the biopolymers and thus promote the decomposition

of biomass. This interpretation is actually in line with the observations by [12], who noted, in the case of potassium, that a certain concentration of  $\rm K_2CO_3$  was needed to weaken the hydrogen bonds and foster the breakage of the glycosidic linkages during the pyrolysis of beech wood. Note also that the catalytic effect induced by  $\rm CaCl_2$  and  $\rm MgCl_2$  seems to progressively vanish when  $\rm C_{cat-i}$  exceeds 0.15 mol  $\rm L^{-1}$ . Indeed, the  $\rm T_{10\%}$  decreases only measure 1.7 ( $\rm CaCl_2$ ) and 8.4 K ( $\rm MgCl_2$ ) when  $\rm C_{cat-i}$  passes from 0.15 to 0.5 mol  $\rm L^{-1}$ , as compared to 21.7 K and 35.4 K when  $\rm C_{cat-i}$  varies from 0 to 0.15 mol  $\rm L^{-1}$ . Similarly,  $\rm T_{max}$  mainly decreases when the concentrations of  $\rm Ca^{2+}$  and  $\rm Mg^{2+}$  increase from 0.05 to 0.3 mol  $\rm L^{-1}$ , after which this temperature tends to plateau. As far as sodium and potassium chlorides are concerned, similar behaviors are globally noted with  $\rm T_{10\%}$  and

Fig. 5 Examples of TG (a, c, e and g) and dTG (b, d, f and h) profiles obtained with a heating rate of 5 K min<sup>-1</sup> for SW samples impregnated with catalyst solutions containing different concentrations (i.e., 025, 0.05, 0.15, 0.3 and 0.5 mol L<sup>-1</sup>) of NaCl (a and b), KCl (c and d), CaCl<sub>2</sub> (e and f) and MgCl<sub>2</sub> (g and h)

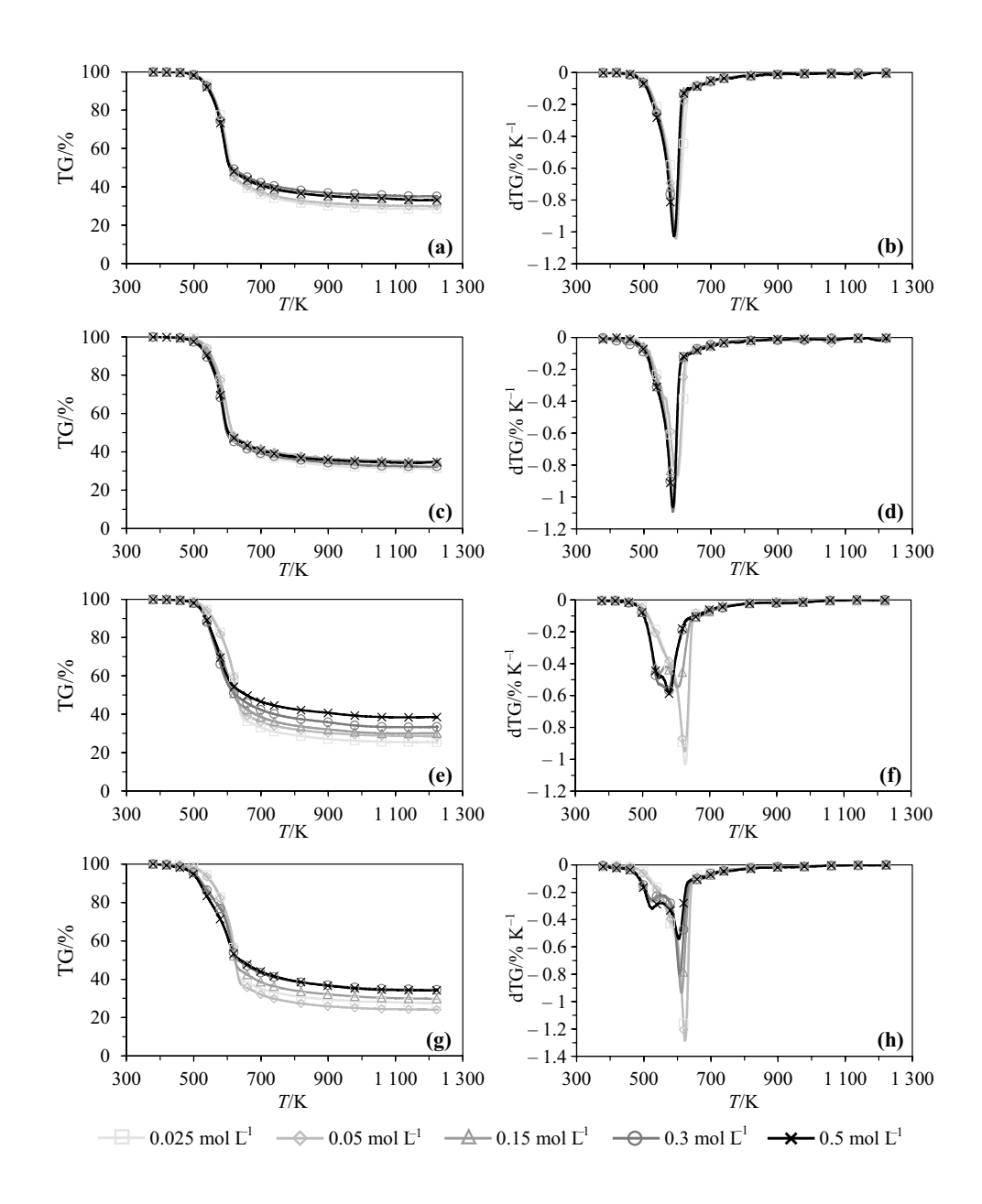




Table 4 Characteristic decomposition temperatures  $(T_{10\%} \text{ and } T_{\text{max}})$ , maximum mass loss rate  $(dTG_{\text{max}})$  and residual mass at 1223 K  $(TG_{1223 \text{ K}})$  measured with raw SW and samples impregnated with catalyst solutions containing different concentrations (denoted  $C_{\text{cat-i}}$ ) of NaCl, KCl, CaCl<sub>2</sub> and MgCl<sub>2</sub> for a heating rate β of 5 K min<sup>-1</sup>. Note that the bracketed values denote the uncertainties (see Sect. "TGA analyses")

$\overline{C_{\mathrm{cat-i}}/\mathrm{mol}\ \mathrm{L}^{-1}}$	T <sub>10%</sub> /K	T <sub>max</sub> /K	d <i>TG</i> <sub>max</sub> /% K <sup>-1</sup>	TG <sub>1223 K</sub>	T <sub>10%</sub> /K	T <sub>max</sub> /K	d <i>TG</i> <sub>max</sub> /% K <sup>-1</sup>	<i>TG</i> <sub>1223 K</sub> /%
	NaCl				KCl			
0	549.5 ( $\pm 0.04$ )	$622.8$ ( $\pm 0.26$ )	-0.88 (± 0.13)	24.9 (±3.43)	$549.5$ ( $\pm 0.04$ )	$622.8$ ( $\pm 0.26$ )	-0.88 (±0.13)	24.9 (±3.43)
0.025	541.7 (±0.97)	603.4 (±0.02)	-0.89 (±0.09)	31.2 (±5.50)	541.1 (±2.09)	$599.0$ ( $\pm 0.23$ )	-0.96 ( $\pm 0.05$ )	31.0 (±3.57)
0.05	538.7 (±0.81)	595.9 (±1.60)	-1.03 (± 0.05)	30.9 (± 2.13)	536.9 (±11.08)	597.4 (±5.83)	-0.95 (±0.18)	34.8 (±1.53)
0.15	$538.4$ ( $\pm 0.12$ )	594.8 (±2.14)	-1.04 (± 0.07)	33.5 (±7.87)	535.8 (± 0.17)	$590.3$ ( $\pm 0.66$ )	-1.15 (±0.11)	$34.7$ ( $\pm 7.05$ )
0.3	$535.6$ ( $\pm 0.83$ )	592.3 (±1.13)	-1.00 ( $\pm 0.03$ )	34.9 (±1.24)	530.3 (±8.10)	588.5 (±3.90)	-1.20 (± 0.21)	33.1 (±1.84)
0.5	$534.3$ ( $\pm 0.50$ )	592.4 (±1.17)	$-1.04$ ( $\pm 0.04$ )	33.0 (±1.45)	530.3 (±4.73)	588.4 (±0.12)	-1.08 ( $\pm 0.02$ )	33.3 (±1.81)
	CaCl <sub>2</sub>				$MgCl_2$			
0	549.5 ( $\pm 0.04$ )	$622.8$ ( $\pm 0.26$ )	-0.88 (± 0.13)	24.9 (±3.43)	$549.5$ ( $\pm 0.04$ )	$622.8$ ( $\pm 0.26$ )	-0.88 (±0.13)	24.9 (±3.43)
0.025	547.2 (±2.52)	627.0 (±0.41)	-1.04 (± 0.02)	26.8 (±3.76)	546.8 (± 0.37)	622.9 (±0.62)	-1.19 (± 0.02)	27.3 (±1.97)
0.05	543.6 (±1.14)	626.1 (±0.59)	-0.97 ( $\pm 0.05$ )	28.4 (±3.53)	541.9 (±3.74)	$620.3$ ( $\pm 5.40$ )	-1.26 (± 0.06)	25.3 (± 2.49)
0.15	527.7 (± 1.46)	605.5 (±3.38)	-0.54 (± 0.02)	30.9 (±1.77)	$514.0$ ( $\pm 0.54$ )	612.7 (± 1.01)	-0.95 ( $\pm 0.03$ )	29.6 (± 0.47)
0.3	$525.6$ ( $\pm 0.14$ )	575.1 (± 1.99)	-0.57 ( $\pm 0.01$ )	33.0 (±0.20)	510.2 (±0.01)	607.3 (± 0.02)	-0.81 (±0.03)	$34.6$ ( $\pm 0.40$ )
0.5	526.0 (±0.19)	579.7 (±0.84)	-0.57 ( $\pm 0.03$ )	36.9 (±2.86)	505.6 (± 0.48)	605.7 (±2.35)	-0.53 (±0.02)	34.8 (±1.32)

 $T_{\rm max}$  reductions, which are mainly observed for  $C_{\rm cat-i} < 0.15~{\rm mol~L^{-1}}$ . Finally, and as can be seen by looking at the  $TG_{1223~{\rm K}}$  values in Table 4, they are shown to increase by  ${\sim}6\%$  when  $C_{\rm cat-i}$  passes from 0 to 0.05 mol  ${\rm L^{-1}}$  for NaCl and KCl, while the residual mass is somewhat constant for higher concentrations (+  ${\sim}2\%$  when  $C_{\rm cat-i}$  increases from 0.05 to 0.5 mol  ${\rm L^{-1}}$ ). Regarding calcium and magnesium, a similar trend is observed, although the cation concentration above which  $TG_{1223~{\rm K}}$  begins to plateau is higher ( ${\sim}0.3~{\rm mol~L^{-1}}$ ). These results thus tend to point to the existence of a saturation phenomenon showing that AAEMs are more efficient in promoting biomass conversion when the  $C_{\rm cat-i}$  values are relatively low.

To further illustrate the presence of this saturating effect from a kinetic perspective, in Fig. 6, we plotted the evolution of the rate constant values computed based on the parameters derived from the implementation of the OFW model as a function of  $C_{\text{cat-i}}$  for T=540~K and SW samples impregnated with NaCl, KCl, CaCl<sub>2</sub> and MgCl<sub>2</sub>. Note that the above temperature of 540 K was selected to plot the  $k=f(C_{\text{cat-i}})$  curves since it is typically comprised within the range of T values (i.e., between  $\sim 500$  and  $\sim 600~\text{K}$ ) on which AAEMs influence pyrolysis kinetics, as evidenced in Sect. "Assessment of rate constant parameters". Note also that since the few studies in the literature that investigated

the effect of AAEMs on pyrolysis kinetics while considering a model-free approach (i.e., [21, 23, 61, 62], to the best of the authors' knowledge) used the OFW method (with the exception of [62], which considered the Friedman approach), the OFW model was therefore chosen to plot the curves in Fig. 6, which will ease potential future comparisons, reiterating that the three isoconversional modeling approaches considered in the present work led to quite similar results (see Sect. "Comparison of simulated and measured conversion degree profiles").

The obtained plots show that the evolution of k as a function of  $C_{\text{cat-i}}$  is roughly asymptotic for concentrations of cations in the impregnating solutions higher than 0.15 mol L<sup>-1</sup>, thus confirming the existence of the above-discussed saturation phenomenon as previously suggested in the literature [12, 21, 63]. [21] indeed reported an asymptotic evolution of k as a function of  $C_{\text{cat-i}}$  during pyrolysis tests performed with beech wood impregnated with CaCl<sub>2</sub> and MgCl<sub>2</sub>. [63] also noted a "leveling off effect" of the apparent first-order reaction rate when pyrolyzing willow treated with different mass percentages of potassium and sodium acetate. According to [33, 66], this phenomenon could be traced to agglomeration issues on the solid surface and to the limited availability of active sites. On the other hand, the curves in Fig. 6 confirm that for a given concentration of cations in the impregnating solution, alkaline earth metals are more efficient



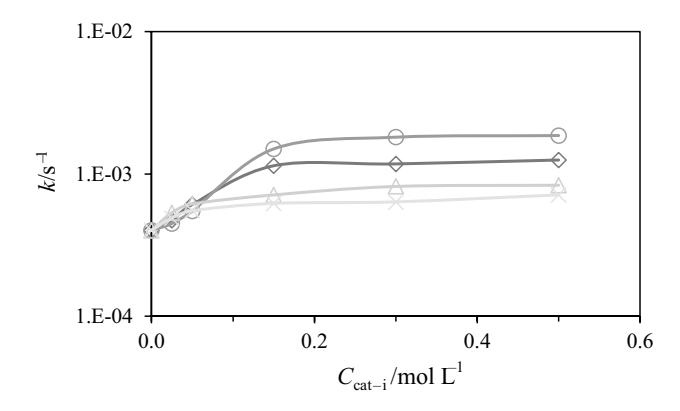


**Fig. 6**  $k = f(C_{\text{cat-i}})$  plots computed using the kinetic parameters issued from the use of the OFW model for T = 540 K and SW samples impregnated with NaCl, KCl, CaCl<sub>2</sub> and MgCl<sub>2</sub>

in increasing the pyrolysis rate constants than alkali ones. The results obtained finally suggest that using high  $C_{\rm cat-i}$  values does not represent the most effective approach for converting biomass into high-value products such as syngas and bio-oils. This statement is particularly supported by the fact that a higher catalyst concentration is accompanied by higher residual masses, as illustrated by the TG curves of Fig. 5. Furthermore, the saturating effect evidenced in Fig. 6 also implies that using impregnating solutions having relatively low catalyst contents (i.e.,  $C_{\rm cat-i}$  not higher than  $\sim 0.15$  mol L<sup>-1</sup>) could represent a more efficient way to convert biomass through the combination of increased reaction rates with limited char production.

To conclude, in Fig. 7, we compare the  $\alpha = f(T)$  profiles measured for  $\beta = 5$  K min<sup>-1</sup> with SW impregnated with two salts containing alkali and alkaline earth metals (i.e., K and Ca as in Fig. 4) for  $C_{\text{cat-i}}$  comprised between 0.025 and 0.5 mol L<sup>-1</sup> with theoretical curves computed using the rate constant parameters obtained from the implementation of the OFW model as an example (see the above comments regarding the similarities observed in terms of results when considering the other isoconversional modeling approaches). The results obtained, here again, show that the predicted

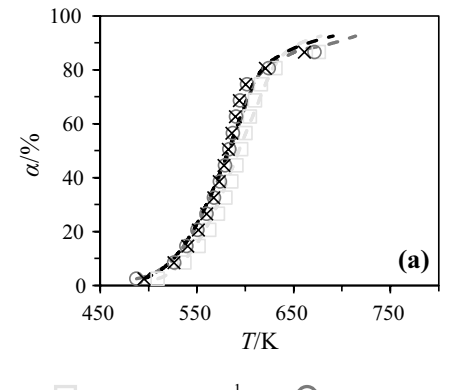
conversion degrees match very well their experimental counterparts. This thus demonstrates that the parameterized model used to plot the profiles of Fig. 7 satisfactorily captures the saturation effect observed based on the TG and dTG curves of Fig. 5, noting that to the best of the authors' knowledge, this phenomenon has seldom been modeled in the literature.

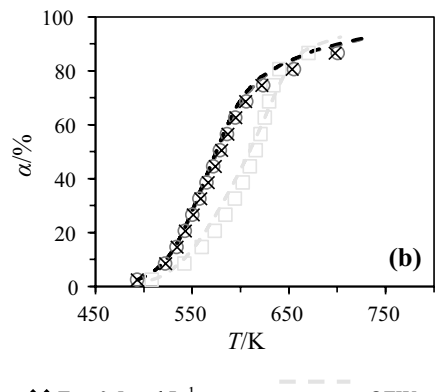
# **Conclusion**

The present work aimed to elucidate the effect of added alkali and alkaline earth metals on the pyrolysis behavior of 5 different feedstocks. Thermogravimetric analyses were conducted using 4 different heating rates (5, 10, 15 and 30 K min<sup>-1</sup>), with raw and catalyzed samples prepared by wet impregnation using 4 AAEM salts, namely NaCl, KCl, CaCl<sub>2</sub> and MgCl<sub>2</sub>. Measured data were processed using the KAS, OFW and Friedman isoconversional methods to infer rate constant parameters which were then used to simulate conversion degree profiles that were compared with measured ones. The following conclusions can be drawn from the results obtained:

• Impregnating SW, M and SG with sodium, potassium, calcium and magnesium chlorides resulted in an overall shift of the pyrolysis process to lower temperatures, as exemplified by significant reductions of T<sub>10%</sub> and T<sub>max</sub>. On the whole, higher decreases of the characteristic pyrolysis temperatures were observed in the case of divalent cations. This higher efficiency of alkaline earth metals in reducing the initial pyrolysis temperatures can notably be traced to their ability to foster the decomposition of hemicellulose and the initial dehydration/decomposition of cellulose, contrary to alkali metals, which are more prone to promote the conversion of cellulose taking place at higher temperatures than the decomposition of hemicellulose. Alternatively, adding NaCl and KCl to WS and SM was shown to induce no significant catalytic effect, due to the high amount of sodium and potas-

**Fig. 7** Comparison of measured and simulated conversion degree profiles obtained with SW impregnated with various concentrations of KCl (**a**) and CaCl<sub>2</sub> (**b**) for a heating rate of 5 K min<sup>-1</sup>





 $\square$  Exp 0.025 mol  $\square$ <sup>-1</sup>

O Exp 0.3 mol L<sup>-1</sup>

 $\times$  Exp 0.5 mol L<sup>-1</sup>

**= = =** OFW



- sium contained in these feedstocks, thus making them less sensitive to further Na and K addition by wet impregnation because of a so-called saturation phenomenon.
- All the tested catalysts were found to increase the residual masses at 1223 K, pointing to the catalytic role played by AAEMs as bridges linking adjacent oxygenated functional groups, thus promoting recombination reactions and char formation.
- Order-based models were shown to be best suited for simulating the pyrolysis of raw and impregnated SW, WS, SM, M and SG samples.
- In agreement with the conclusions drawn in our recent benchmarking analysis which set out to assess the ability of 7 modeling approaches to infer rate constant parameters that were appropriate for simulating the pyrolysis of different types of biomasses [24], the Friedman differential method provided the best agreement between experimental and theoretical  $\alpha = f(T)$  plots. It was followed by the KAS and OFW models. The KAS and OFW methods were still shown to lead to very consistent results, with mean root-mean-square deviations between measured and simulated  $\alpha = f(T)$  profiles never exceeding 3.5%.
- The analysis of the kinetic parameters obtained using the KAS, OFW and Friedman models showed that adding CaCl2 and MgCl2 to SW, WS, M and SG induced significant increases of the rate constants over a 500 to 600 K temperature range. On the other hand, and while reducing the activation energies assessed in the case of SW and WS as examples, the effect of NaCl and KCl on the rate constant values was found to be much weaker, especially for WS, whose high inherent K and Na contents cause this sample to be less influenced by the addition of further potassium and sodium. Furthermore, none of the tested catalysts was found to truly promote the pyrolysis of SM, which has been traced to the low hemicellulose and cellulose and high inherent AAEM contents of this biomass. Finally, the fact that alkaline earth metals were shown to exhibit a stronger ability to increase the pyrolysis rates as compared to alkali metals for 500 K < T < 600 K was explained by the fact that the former are more prone to weaken the strength of the intramolecular bonds of biopolymers, thereby facilitating the decomposition of biomass at low temperatures.

• The sensitivity analysis focusing on the impact of the catalyst load on the pyrolysis kinetics of SW demonstrated a saturation phenomenon characterized by the absence of additional reductions of T<sub>10%</sub> and T<sub>max</sub> in addition to rather negligible variations of k when the concentration of cations in the impregnating solutions exceeds a critical value (estimated as being ~0.15 mol L<sup>-1</sup>). This observation thus contributes to demonstrating that the relative efficiency of AAEMs in promoting the conversion of biomass tends to be higher when the catalysts are used at relatively low contents.

In conclusion, the present work contributes to elucidating the catalytic effect induced by different AAEMs added to a wide variety of biomass types. While exemplifying the effect of some metal salts on the increase of the rate constants accounting for the decomposition of hemicellulose and cellulose, this research is also one of the few which demonstrates the existence of the socalled saturation phenomenon (whose detailed mechanisms still need to be further explored) through a complete kinetic modeling of measured TGA data using isoconversional approaches. Additional investigations should, however, be conducted to better elucidate the mechanisms involved in the AAEM-catalyzed pyrolysis of biomass. A fine characterization of the distribution of the catalysts within the biomass components would notably be of interest to gain further information on how the interactions between the metal cations and the biopolymers may influence pyrolysis kinetics. Furthermore, and based on the findings reported herein regarding the AAEM catalysts, which are more effective at promoting the decomposition of biomass, and the cation concentrations in the impregnating solution, which should be preferentially selected for an optimal conversion of the treated feedstocks, complementary pyrolysis tests conducted at a larger scale, using an auger reactor, for instance, should be helpful to further improve our understanding of the pyrolysis features of AAEM-catalyzed solid fuels, thus paving the way for future works.

# **Appendix**

See Table A1.



**Table A1** Characteristic pyrolysis temperatures  $(T_{10\%}, T_{50\%}, T_{90\%})$  and  $T_{\rm max}$ , maximal mass loss rates  $(dTG_{\rm max})$  and residual mass at 1223 K  $(TG_{1223~\rm K})$  measured with raw SW, WS, SM, M and SG and samples

impregnated with NaCl, KCl,  $CaCl_2$  and  $MgCl_2$ . Note that the bracketed values denote the uncertainties (see Sect. "TGA analyses")

Sam	ple	T <sub>10%</sub> /K	T <sub>50%</sub> /K	T <sub>90%</sub> /K	T <sub>max</sub> /K	d <i>TG</i> <sub>max</sub> /% K <sup>−1</sup>	<i>TG</i> <sub>1223 K</sub> /%	T <sub>10%</sub> /K	T <sub>50%</sub> /K	T <sub>90%</sub> /K	T <sub>max</sub> /K	d <i>TG</i> <sub>max</sub> /% K <sup>-1</sup>	<i>TG</i> <sub>1223 K</sub> /%
		5 K min	-1					10 K mir	n <sup>-1</sup>				
SW	Raw	$549.5$ ( $\pm 0.04$ )	609.5 (±0.37)	700.7 $(\pm 1.29)$	$622.8$ ( $\pm 0.26$ )	-0.88 (±0.13)	24.9 (±3.43)	566.3 (±0.89)	626.9 (± 0.9)	730.0 $(\pm 5.18)$	639.4 (±0.97)	-0.96 (±0.02)	22.5 (± 0.62)
	NaCl	$538.4$ ( $\pm 0.12$ )	589.8 (±1.51)	718.3 $(\pm 1.42)$	594.8 (±2.14)	$-1.04$ ( $\pm 0.07$ )	33.5 (±5.87)	$551.8$ ( $\pm 0.54$ )	605.3 (±0.97)	735.4 (±3.54)	$610.7$ ( $\pm 0.85$ )	-1.04 (± 0.05)	32.4 (±2.56)
	KCl	535.8 (±0.17)	585 (± 0.83)	698.2 (±5.24)	590.3 (±0.66)	-1.15 (±0.11)	34.7 (±4.05)	$549.8$ ( $\pm 0.64$ )	601.3 (±0.61)	719.7 (±0.21)	606.7 (±0.72)	-1.14 (± 0.02)	31.7 (±1.03)
	CaCl <sub>2</sub>	527.7 (±1.46)	591.4 (±1.5)	721.0 (±2.37)	605.5 (±3.38)	-0.54 (±0.02)	30.9 (±1.77)	539.6 (±0.34)	599.9 (±0.64)	741.6 (± 0.21)	601.9 (±0.82)	-0.50 ( $\pm 0.01$ )	29.9 (±1.21)
	$MgCl_2$	514.0 (±0.54)	605.1 (±0.11)	729.5 (±7.27)	612.7 (±1.01)	-0.95 ( $\pm 0.03$ )	29.6 (±0.47)	524.7 (±0.19)	617.3 (±0.16)	739.6 (±1.49)	625.6 (±0.11)	-0.87 ( $\pm 0.04$ )	29.8 (±2.95)
WS	Raw	$525.7$ ( $\pm 0.03$ )	$576.7$ ( $\pm 0.20$ )	728.0 (± 0.99)	577.4 (±0.86)	-0.82 ( $\pm 0.02$ )	34.9 (±0.11)	$540.0$ ( $\pm 2.46$ )	591.0 (±2.98)	744.3 (±2.99)	591.9 (±3.50)	$-0.83$ ( $\pm 0.06$ )	34.2 (±5.13)
	NaCl	531.0 (±1.06)	580.0 (± 0.02)	727.1 (±4.95)	584.0 (±0.32)	-0.84 (± 0.04)	42.2 (±3.97)	545.0 (±0.29)	594.3 (±0.19)	739.0 (±3.64)	598.7 (±0.16)	-0.72 (± 0.14)	50.3 (±4.36)
	KCl	529.5 (± 0.68)	579.7 (±0.58)	748.4 (± 1.41)	582.7 (±0.19)	-0.78 (±0.27)	44.4 (±5.83)	543.3 (±1.49)	593.7 (±0.46)	759.0 (±1.31)	597.1 (±0.78)	-0.61 (± 0.03)	56.2 (± 2.08)
	CaCl <sub>2</sub>	512.6 (±0.13)	572.9 (±0.87)	756.6 (± 1.9)	575.4 (±1.03)	-0.57 ( $\pm 0.14$ )	44.8 (±3.55)	524.9 (±0.59)	581.4 (±0.02)	767.8 (± 3.19)	582.4 (±0.34)	-0.62 (±0.05)	41.3 (±3.78)
	MgCl <sub>2</sub>	495.0 (±0.57)	582.5 (±0.17)	741.8 (±4.91)	592.2 (±0.08)	-0.54 (±0.03)	40.4 (±5.63)	507.0 (± 0.29)	593.8 (± 0.8)	755.7 (±4.72)	604.3 (±1.22)	-0.48 (± 0.05)	42.1 (±10.33)
SM	Raw	505.5 (±0.37)	582.2 (±0.34)	904.2 (±3.15)	582.9 (±1.26)	-0.43 (±0.01)	39.7 (±1.21)	520.1 (±0.83)	596.4 (± 0.8)	919.8 (± 0.02)	596.9 (±1.11)	-0.42 (± 0.01)	37.6 (± 0.05)
	NaCl	507.3 (± 0.03)	583.2 (±0.12)	926.2 (±4.66)	583.0 (±0.15)	-0.45 ( $\pm 0.00$ )	36.7 (±0.12)	519.8 (±0.07)	596.6 (±0.11)	938.1 (±6.01)	596.0 (± 2.1)	-0.44 (± 0.02)	35.9 (±1.39)
	KCl	508.5 (± 0.06)	577.9 (± 1.08)	893.3 (±8.93)	578.5 (± 0.64)	-0.44 (± 0.02)	37.6 (± 0.44)	522.0 (±0.57)	591.6 (±0.84)	910.3 (±3.42)	592.8 (±0.16)	-0.43 (± 0.01)	37.9 (± 1.34)
	CaCl <sub>2</sub>	492.9 (±0.32)	578.7 (±0.69)	872.2 (±4.56)	570.9 (±2.51)	-0.30 ( $\pm 0.04$ )	39.2 (± 2.63)	506.5 (± 0.68)	590.3 (± 0.97)	891.4 (±3.55)	579.5 (±1.81)	-0.31 (±0.01)	38.8 (± 0.86)
	$MgCl_2$	483.4 (±1.08)	581.8 (± 0.75)	885.2 (± 1.61)	574.9 (±2.47)	-0.28 ( $\pm 0.02$ )	40.4 (± 2.53)	497.3 (±0.31)	594.1 (±0.36)	905.9 (± 0.93)	584.5 (±0.34)	-0.26 (± 0.01)	42.3 (±1.61)
M	Raw	535.2 (± 0.08)	598.1 (±0.16)	713.6 (±1.31)	612.0 (± 1.07)	-0.75 (±0.01)	31.2 (± 0.48)	549.6 (±0.31)	611.9 (±0.06)	724.2 (±4.35)	626.5 (± 0.19)	-0.65 ( $\pm 0.10$ )	33.6 (±4.34)
	NaCl	529.9 (±0.56)	593.1 (±0.37)	833.8 (±5.39)	599.3 (±0.57)	-0.81 (± 0.02)	43.4 (±2.12)	544.2 (± 0.24)	608.1 (±0.19)	873.6 (±5.18)	613.9 (±0.04)	-0.80 ( $\pm 0.06$ )	40.8 (± 4.98)
	KCl	527 (±0.21)	590.7 (±0.19)	847.4 (±6.18)	596.3 (±0.05)	-0.81 (±0.06)	42.4 (±1.33)	540.9 (±0.27)	605.3 (±0.29)	869.9 (±5.99)	611.1 (±0.21)	-0.76 ( $\pm 0.02$ )	44.2 (± 0.85)
	CaCl <sub>2</sub>	500.2 (± 1.25)	569.2 (±1.41)	738.6 (± 3.06)	574.5 (±1.40)	-0.40 ( $\pm 0.08$ )	54.9 (±8.56)	511.5 (±0.01)	580.4 (±1.56)	756.1 $(\pm 2.98)$	584.4 (±2.59)	-0.36 (±0.07)	57.9 (±7.78)
	$MgCl_2$	488.3 (± 1.78)	580.9 (±0.93)	729.5 (±1.15)	593.1 (±0.10)	-0.62 (±0.04)	39.6 (±5.36)	500.4 (±2.84)	592.6 (±2.09)	742.6 (±5.18)	603.1 (±5.18)	-0.52 (±0.06)	44.7 (±6.99)
SG	Raw	534.6 (±0.62)	599.7 (±1.06)	718.0 $(\pm 0.85)$	613.8 (±0.49)	-0.75 ( $\pm 0.08$ )	29.1 (±4.02)	549.6 (±0.24)	614.3 (±0.36)	734.0 (±4.39)	$629.2$ ( $\pm 0.23$ )	-0.68 (±0.13)	29.3 (±3.66)
	NaCl	$526.7$ ( $\pm 0.93$ )	591.9 (±0.80)	747.8 (±8.79)	599.5 (±1.07)	-0.85 ( $\pm 0.04$ )	29.6 (±5.92)	540.5 (±0.31)	606.3 (±0.26)	753.2 (±0.89)	614.9 (±0.27)	-0.82 (± 0.04)	31.4 (±3.49)
	KCl	523.5 (±0.76)	587.7 (±0.98)	752.4 (±4.98)	594.7 (±1.00)	-0.80 ( $\pm 0.02$ )	31.5 (±0.53)	538.3 (±0.19)	602.3 (± 0.52)	771.3 (±2.61)	609.4 (± 0.68)	-0.80 ( $\pm 0.03$ )	30 (±2.07)
	CaCl <sub>2</sub>	507.1 (±0.21)	582.8 (± 0.10)	$714.7$ ( $\pm 0.58$ )	595.9 (±1.50)	-0.58 ( $\pm 0.02$ )	34.8 (±0.19)	519.4 (±0.01)	$594.8$ ( $\pm 0.33$ )	729.6 $(\pm 2.67)$	611.7 (±4.17)	-0.54 (± 0.04)	34.1 (±0.35)
	$MgCl_2$	488.6 (±1.83)	$582.3$ ( $\pm 0.80$ )	732.7 $(\pm 2.30)$	592.8 (±2.81)	-0.63 ( $\pm 0.04$ )	34.0 (±1.92)	501.0 (± 3.50)	594.2 (±2.29)	746.4 (±5.11)	603.0 (±3.91)	-0.53 ( $\pm 0.01$ )	39.2 (±5.15)



Table A1 (continued)

Sample		T <sub>10%</sub> /K	$T_{50\%}$ /K	T <sub>90%</sub> /K	$T_{ m max}$ /K	$dTG_{max}$ /% $K^{-1}$	<i>TG</i> <sub>1223 K</sub> /%	T <sub>10%</sub> /K	T <sub>50%</sub> /K	$T_{90\%}$ /K	$T_{ m max}$ /K	$dTG_{max}$ /% $K^{-1}$	$TG_{1223 \text{ K}}$	
		15 K mir		/11	/11	770 11	770	30 K min <sup>-1</sup>						
SW	Raw	575.6 (±2.17)	635.7 (±1.45)	730.1 (±6.92)	648.4 (±1.22)	-0.89 (±0.07)	24.6 (±4.35)	598.3 (±2.76)	657.1 (±2.22)	743.4 (±1.06)	667.9 (±2.28)	-0.88 (±0.01)	25.9 (±1.83)	
	NaCl	563.2 (± 0.86)	617.7 (±0.67)	747.4 (± 2.01)	622.9 (± 0.6)	-1.05 ( $\pm 0.02$ )	32.2 (± 0.57)	584.4 (±1.46)	639.2 (± 0.52)	765.6 (± 5.04)	642.5 (± 0.43)	-0.92 (±0.01)	33.4 (±0.91)	
	KCl	561.3 (± 0.41)	613.2 (± 0.65)	728.8 (± 2.12)	618.4 (±0.47)	-1.13 (±0.01)	31.0 (± 0.76)	584.4 (± 1.51)	635.8 (± 0.9)	747.2 (±0.25)	639.4 (±0.77)	-1.02 (± 0.01)	30.9 (±0.33)	
	CaCl <sub>2</sub>	549.0 (± 0.74)	606.4 (± 0.33)	756.3 $(\pm 1.48)$	602.7 (±0.7)	-0.53 (±0.01)	30.0 (± 1.18)	567.9 (± 1.64)	620.5 (± 1.72)	775.6 $(\pm 0.68)$	612.7 (± 2.12)	-0.61 (±0.01)	31.2 (±0.09)	
	MgCl <sub>2</sub>	533.5 (± 0.53)	625.5 (± 0.42)	$750.4$ ( $\pm 0.42$ )	634.3 (±0)	-0.82 (±0.01)	29.5 (±0.84)	550.9 (± 0.66)	643.3 (± 0.94)	765.1 $(\pm 7.23)$	653.1 (± 1.26)	-0.59 ( $\pm 0.04$ )	39.8 (± 3.35)	
WS	Raw	551.8 (±1.27)	602.1 (±0.65)	748.8 (± 2.92)	602.9 (± 0.12)	-0.86 (±0.01)	32.8 (±0.49)	572.1 (± 2.06)	621.9 (± 2.04)	765.7 (± 3.46)	620.5 (± 2.1)	-0.82 (±0.03)	35.0 (±0.12)	
	NaCl	$558.3$ ( $\pm 0.35$ )	607.0 (± 0.24)	752.6 $(\pm 5.63)$	610.9 (±0.23)	-0.91 (±0.07)	36.7 (±5.36)	581.0 (±2.04)	629.4 (±2.01)	771.1 (±5.82)	631.1 (±2.24)	-0.81 (±0.19)	40.0 (± 6.36)	
	KCl	555.1 (±0.33)	605.0 (±0.37)	775.3 (±3.68)	607.7 (± 0.43)	-0.75 (±0.11)	46.1 (±6.28)	579.0 (±0.1)	628.1 (± 0.18)	795.2 (±1.71)	628.7 (± 0.3)	-0.84 (±0.07)	36.5 (±5.29)	
	CaCl <sub>2</sub>	535.1 (±0.11)	589.5 (±0.88)	778.5 $(\pm 0.52)$	589.9 (±1.19)	-0.54 (±0.08)	49.7 (±4.07)	552.5 (±0.20)	604.9 (±0.74)	793.2 (± 1.13)	602.6 (±0.81)	-0.61 (±0.03)	43.4 (±2.66)	
	$MgCl_2$	516.5 (±0.66)	600.6 (± 1.2)	765.0 (± 3.11)	610.1 (±2.50)	$-0.44$ ( $\pm 0.05$ )	41.7 (±7.42)	532.2 (±1.05)	614.3 (±0.27)	782.8 (± 0.05)	618.4 (±0.05)	-0.40 ( $\pm 0.04$ )	41.4 (±5.45)	
SM	Raw	531.8 (±0.66)	605.3 (± 0.43)	934.3 (±5.33)	605.6 (± 0.32)	-0.42 (±0.01)	36.9 (±0.01)	547.7 (±0.11)	627.6 (± 0.92)	962.1 (±4.58)	626.7 (± 0.28)	-0.42 (±0.01)	36.1 (±0.77)	
	NaCl	533.2 (± 0.10)	607.3 (±0.16)	949.7 (±4.85)	607.8 (± 0.08)	-0.44 (± 0.01)	36.3 (±0.31)	547.3 (± 0.09)	$630.3$ ( $\pm 0.18$ )	972.4 (±5.69)	628.9 (± 0.87)	-0.44 (± 0.03)	35.7 (± 2.51)	
	KCl	534.5 (± 0.59)	601.9 (±0.19)	916.7 (±6.48)	603.6 (±0.03)	-0.43 (±0.01)	37.8 (± 1.04)	549.3 (± 1.52)	626.1 (± 1.54)	957.0 (±0.31)	625.2 (± 1.41)	-0.41 (± 0.02)	37.6 (± 2.96)	
	CaCl <sub>2</sub>	518.4 (±0)	599.9 (± 0.25)	900.2 (± 2.99)	583.3 (± 3.1)	-0.29 (±0.01)	39.3 (±0.32)	533.4 (±0.74)	619.9 (±0.49)	920.0 $(\pm 2.86)$	599.2 (±0.01)	-0.33 (±0.01)	38.7 (± 1.21)	
	MgCl <sub>2</sub>	504.9 (± 0.82)	603.8 (± 1.41)	919.4 (±6.68)	588 (±6.01)	-0.26 (±0.01)	37.5 (± 5.81)	$525.6$ ( $\pm 0.82$ )	$624.5$ ( $\pm 0.78$ )	940.6 (±3.61)	600.5 (± 1.93)	-0.27 (±0.01)	43.6 (± 2.95)	
M	Raw	564.9 (±2.12)	626.9 (±1.41)	742.4 (± 1.97)	640.8 (± 0.77)	-0.72 (± 0.04)	31.1 (±1.02)	589.3 (±2.99)	649.1 (± 3.75)	758.6 $(\pm 3.42)$	661.8 (±3.91)	-0.68 (±0.02)	31.0 (±0.19)	
	NaCl	554.5 (± 0.15)	618.4 (± 0.34)	884.2 (± 2.35)	624.1 (± 0.21)	-0.82 (± 0.02)	38.1 (± 1.56)	576.0 (± 1.09)	639.1 (±0.69)	928.5 (±1.31)	$643.6$ ( $\pm 0.48$ )	-0.73 (±0.09)	36.1 (± 5.87)	
	KCl	551.4 (±0.21)	615.6 (±0.11)	894.8 (±13.71)	621.2 (±0.29)	-0.82 (± 0.05)	37.6 (± 3.42)	571.7 (±0.68)	635.3 (±0.21)	936.9 (±2.85)	639.5 (±0.21)	-0.67 (± 0.04)	41.3 (± 3.2)	
	CaCl <sub>2</sub>	522.6 (±0.92)	586.8 (±1.12)	770.5 $(\pm 4.88)$	589.7 (±1.01)	-0.41 (± 0.04)	50.9 (±5.21)	536.0 (±1.68)	604.6 (±4.87)	795.6 (± 0.32)	602.8 (±3.89)	-0.45 (±0.13)	50.5 (± 6.52)	
	MgCl <sub>2</sub>	507.6 (±0.99)	600.6 (± 0.65)	754.6 (± 2.27)	613.5 (± 0.42)	-0.49 (±0.01)	43.2 (±1.26)	525.9 (±0.95)	621.0 (±2.01)	773.8 (±3.38)	634.7 (±5.33)	-0.42 (±0.02)	43.9 (±3.05)	
SG	Raw	563.0 (±1.32)	626.9 (±0.27)	756.3 (± 2.90)	641.2 (±1.32)	-0.65 (±0.03)	29.1 (±3.27)	586.7 (±0.35)	649.1 (±0.18)	788.2 (±1.91)	661.7 (±0.15)	-0.65 (±0.01)	27.5 (±0.14)	
	NaCl	551.7 (±0.65)	617.6 (±1.02)	768.7 (± 2.54)	625.5 (±0.72)	-0.85 (± 0.03)	27.0 (± 1.13)	571.7 (±1.39)	637.3 (±0.88)	795.5 (±1.7)	644.2 (±0.63)	-0.75 (±0.01)	$(\pm 0.86)$	
	KCl	549.7 (±1.76)	613.1 (±0.97)	797.4 (±0.4)	619.6 (±0.03)	-0.76 (±0.01)	31.7 (±0.29)	570.5 (±0.67)	634.5 (±0.04)	821.6 (±0.66)	640.6 (±0.17)	-0.64 (±0.1)	35.5 (±5.75)	
	CaCl <sub>2</sub>	531.8 (±0.12)	603.5 (±1.05)	741.1 $(\pm 3.65)$	614.8 (±4.68)	-0.51 (±0.01)	32.6 (± 0.78)	544.9 (±0.38)	623.4 (±0.59)	768.2 (± 6.81)	630.3 (±0.61)	-0.45 (±0.05)	34.9 (±0.23)	
	MgCl <sub>2</sub>	507.2 (± 1.97)	601.5 (± 1.39)	757.8 (± 5.03)	610.8 (± 2.76)	-0.50 ( $\pm 0.03$ )	38.3 (± 6.41)	526.3 (± 0.43)	622.7 (± 0.56)	773.0 $(\pm 6.25)$	631.1 (±0.91)	$-0.43$ ( $\pm 0.01$ )	42.0 (± 1.50)	



Acknowledgement This research was supported by the Natural Sciences and Engineering Research Council of Canada (NSERC). Furthermore, the authors thank Stephane Godbout, Joahnn Palacios and Laura Daniela Mila Saavedra from the Research and Development Institute for the Agri-Environment (IRDA) in Quebec for providing the tested biomass as well as for performing the proximate, ultimate, biopolymer content and inorganic content analyses.

**Author Contributions** Conceptualization, methodology, funding acquisition, project administration, supervision, validation and writing—review and editing were done by R.L.; investigation, formal analysis, visualization and writing—original draft preparation were done by O.F. and R.L.; resources were done by R.L. and A.B.

Funding Natural Sciences and Engineering Research Council of Canada, RGPIN-2023-03300, Romain Lemaire

Open Access This article is licensed under a Creative Commons Attribution-NonCommercial-NoDerivatives 4.0 International License, which permits any non-commercial use, sharing, distribution and reproduction in any medium or format, as long as you give appropriate credit to the original author(s) and the source, provide a link to the Creative Commons licence, and indicate if you modified the licensed material. You do not have permission under this licence to share adapted material derived from this article or parts of it. The images or other third party material in this article are included in the article's Creative Commons licence, unless indicated otherwise in a credit line to the material. If material is not included in the article's Creative Commons licence and your intended use is not permitted by statutory regulation or exceeds the permitted use, you will need to obtain permission directly from the copyright holder. To view a copy of this licence, visit http://creativecommons.org/licenses/by-nc-nd/4.0/.

# References

- Kabir G, Hameed BH. Recent progress on catalytic pyrolysis of lignocellulosic biomass to high-grade bio-oil and bio-chemicals. Renew Sustain Energy Rev. 2017;70:945–67. https://doi.org/10. 1016/j.rser.2016.12.001.
- Chen X, Che Q, Li S, Liu Z, Yang H, Chen Y, et al. Recent developments in lignocellulosic biomass catalytic fast pyrolysis: strategies for the optimization of bio-oil quality and yield. Fuel Process Technol. 2019;196:106180. https://doi.org/10.1016/j.fuproc.2019. 106180.
- 3. Qiu B, Tao X, Wang J, Liu Y, Li S, Chu H. Research progress in the preparation of high-quality liquid fuels and chemicals by catalytic pyrolysis of biomass: a review. Energy Convers Manag. 2022;261:115647. https://doi.org/10.1016/j.enconman.2022.115647.
- Wang W, Lemaire R, Bensakhria A, Luart D. Review on the catalytic effects of alkali and alkaline earth metals (AAEMs) including sodium, potassium, calcium and magnesium on the pyrolysis of lignocellulosic biomass and on the co-pyrolysis of coal with biomass. J Anal Appl Pyrolysis. 2022;163:105479. https://doi.org/10.1016/j.jaap.2022.105479.
- Zhao N, Li B-X. The effect of sodium chloride on the pyrolysis of rice husk. Appl Energy. 2016;178:346–52. https://doi.org/10. 1016/j.apenergy.2016.06.082.
- Chen M, Wang J, Zhang M, Chen M, Zhu X, Min F, et al. Catalytic effects of eight inorganic additives on pyrolysis of pine wood sawdust by microwave heating. J Anal Appl Pyrolysis. 2008;82:145–50. https://doi.org/10.1016/j.jaap.2008.03.001.

- Jensen A, Dam-Johansen K, Wójtowicz MA, Serio MA. Tg-ftir study of the influence of potassium chloride on wheat straw pyrolysis. Energy Fuels. 1998. https://doi.org/10.1021/ef980008i.
- Patwardhan PR, Satrio JA, Brown RC, Shanks BH. Influence of inorganic salts on the primary pyrolysis products of cellulose. Bioresour Technol. 2010;101:4646–55. https://doi.org/10.1016/j. biortech.2010.01.112.
- Leng E, Wang Y, Gong X, Zhang B, Zhang Y, Xu M. Effect of KCl and CaCl2 loading on the formation of reaction intermediates during cellulose fast pyrolysis. Proc Combust Inst. 2017;36:2263– 70. https://doi.org/10.1016/j.proci.2016.06.167.
- Wang Z, Wang F, Cao J, Wang J. Pyrolysis of pine wood in a slowly heating fixed-bed reactor: Potassium carbonate versus calcium hydroxide as a catalyst. Fuel Process Technol. 2010;91:942– 50. https://doi.org/10.1016/j.fuproc.2009.09.015.
- Nowakowski DJ, Jones JM, Brydson RMD, Ross AB. Potassium catalysis in the pyrolysis behaviour of short rotation willow coppice. Fuel. 2007;86:2389

  402. https://doi.org/10.1016/j.fuel.2007. 01.026
- Richa L, Colin B, Pétrissans A, Wallace C, Hulette A, Quirino RL, et al. Catalytic and char-promoting effects of potassium on lignocellulosic biomass torrefaction and pyrolysis. Environ Technol Innov. 2023;31:103193. https://doi.org/10.1016/j.eti.2023.103193.
- Shimada N, Kawamoto H, Saka S. Different action of alkali/ alkaline earth metal chlorides on cellulose pyrolysis. J Anal Appl Pyrolysis. 2008;81:80–7. https://doi.org/10.1016/j.jaap.2007.09. 005.
- Veses A, Aznar M, Martínez I, Martínez JD, López JM, Navarro MV, et al. Catalytic pyrolysis of wood biomass in an auger reactor using calcium-based catalysts. Bioresour Technol. 2014;162:250–8. https://doi.org/10.1016/j.biortech.2014.03.146.
- Sun L, Zhang X, Chen L, Zhao B, Yang S, Xie X. Effects of Fe contents on fast pyrolysis of biomass with Fe/CaO catalysts. J Anal Appl Pyrolysis. 2016;119:133–8. https://doi.org/10.1016/j. jaap.2016.03.008.
- Chen X, Chen Y, Yang H, Chen W, Wang X, Chen H. Fast pyrolysis of cotton stalk biomass using calcium oxide. Bioresour Technol. 2017;233:15–20. https://doi.org/10.1016/j.biortech.2017.02.070
- Chireshe F, Collard F-X, Görgens J. Production of an upgraded bio-oil with minimal water content by catalytic pyrolysis: Optimisation and comparison of CaO and MgO performances. J Anal Appl Pyrolysis. 2019;146:104751. https://doi.org/10.1016/j.jaap. 2019.104751.
- Kawamoto H, Yamamoto D, Saka S. Influence of neutral inorganic chlorides on primary and secondary char formation from cellulose. J Wood Sci. 2008;54:242–6. https://doi.org/10.1007/s10086-007-0930-8.
- Hwang H, Oh S, Choi I-G, Choi JW. Catalytic effects of magnesium on the characteristics of fast pyrolysis products bio-oil, bio-char, and non-condensed pyrolytic gas fractions. J Anal Appl Pyrolysis. 2015;113:27–34. https://doi.org/10.1016/j.jaap.2014.09.028.
- Chen Y, Zhang Y, Yang H, Zhang H, Zhang S, Chen H. Influence of interaction between biomass inorganic components and volatiles on corncob pyrolysis and char structure. Fuel Process Technol. 2022;235:107360. https://doi.org/10.1016/j.fuproc.2022.107360.
- Wang W, Lemaire R, Bensakhria A, Luart D. Analysis of the catalytic effects induced by alkali and alkaline earth metals (AAEMs) on the pyrolysis of Beech wood and corncob. Catalysts. 2022;12:1505. https://doi.org/10.3390/catal12121505.
- Wang W, Lemaire R, Bensakhria A, Luart D. Thermogravimetric analysis and kinetic modeling of the AAEM-catalyzed pyrolysis



- of woody biomass. Molecules. 2022;27:7662. https://doi.org/10.3390/molecules27227662.
- Wang M, Zhang S, Liu X, Ma Y, Wang J. Catalytic co-pyrolysis of cellulose over alkali and alkaline earth metal salts for levoglucosan production. Ind Crops Prod. 2023;201:116925. https://doi. org/10.1016/j.indcrop.2023.116925.
- Fischer O, Lemaire R, Bensakhria A. Thermogravimetric analysis and kinetic modeling of the pyrolysis of different biomass types by means of model-fitting, model-free and network modeling approaches. J Therm Anal Calorim. 2024. https://doi.org/10.1007/ s10973-023-12868-w.
- Vyazovkin S, Chrissafis K, Di Lorenzo ML, Koga N, Pijolat M, Roduit B, et al. ICTAC kinetics committee recommendations for collecting experimental thermal analysis data for kinetic computations. Thermochim Acta. 2014;590:1–23. https://doi.org/10. 1016/j.tca.2014.05.036.
- Wang J, Zhang M, Chen M, Min F, Zhang S, Ren Z, et al. Catalytic effects of six inorganic compounds on pyrolysis of three kinds of biomass. Thermochim Acta. 2006;444:110–4. https://doi.org/10.1016/j.tca.2006.02.007.
- Yu Y, Liu D, Wu H. Formation and characteristics of reaction intermediates from the fast pyrolysis of NaCl- and MgCl<sub>2</sub>-loaded celluloses. Energy Fuels. 2014;28:245–53. https://doi.org/10. 1021/ef401483u.
- Wang W-L, Ren X-Y, Li L-F, Chang J-M, Cai L-P, Geng J. Catalytic effect of metal chlorides on analytical pyrolysis of alkali lignin. Fuel Process Technol. 2015;134:345–51. https://doi.org/10.1016/j.fuproc.2015.02.015.
- Haddad K, Jeguirim M, Jellali S, Guizani C, Delmotte L, Bennici S, et al. Combined NMR structural characterization and thermogravimetric analyses for the assessment of the AAEM effect during lignocellulosic biomass pyrolysis. Energy. 2017;134:10–23. https://doi.org/10.1016/j.energy.2017.06.022.
- 30. Feng D, Zhang Y, Zhao Y, Sun S. Catalytic effects of ion-exchangeable K+ and Ca2+ on rice husk pyrolysis behavior and its gas-liquid-solid product properties. Energy. 2018;152:166–77. https://doi.org/10.1016/j.energy.2018.03.119.
- Lin X, Kong L, Cai H, Zhang Q, Bi D, Yi W. Effects of alkali and alkaline earth metals on the co-pyrolysis of cellulose and high density polyethylene using TGA and Py-GC/MS. Fuel Process Technol. 2019;191:71–8. https://doi.org/10.1016/j.fuproc.2019. 03.015.
- Safar M, Lin B-J, Chen W-H, Langauer D, Chang J-S, Raclavska H, et al. Catalytic effects of potassium on biomass pyrolysis, combustion and torrefaction. Appl Energy. 2019;235:346–55. https:// doi.org/10.1016/j.apenergy.2018.10.065.
- 33. Guo F, Liu Y, Wang Y, Li X, Li T, Guo C. Pyrolysis kinetics and behavior of potassium-impregnated pine wood in TGA and a fixed-bed reactor. Energy Convers Manag. 2016;130:184–91. https://doi.org/10.1016/j.enconman.2016.10.055.
- Zhou W, Bai B, Chen G, Ma L, Jing D, Yan B. Study on catalytic properties of potassium carbonate during the process of sawdust pyrolysis. Int J Hydrogen Energy. 2018;43:13829–41. https://doi. org/10.1016/j.ijhydene.2018.02.002.
- Bach-Oller A, Furusjö E, Umeki K. On the role of potassium as a tar and soot inhibitor in biomass gasification. Appl Energy. 2019;254:113488. https://doi.org/10.1016/j.apenergy.2019. 113488.
- Khopkar SM. Basic concepts of analytical chemistry. New Age International; 1998.
- Hamim N, Aristiawan Y, Hindayani A, Andreas KI. Method verification for determination of sodium chloride purity: A comparison of potentiometric and mohr titration. AIP Conf Proc. 2023;2902:020005. https://doi.org/10.1063/5.0173420.
- Wang W, Lemaire R, Bensakhria A, Luart D. Thermogravimetric analysis and kinetic modeling of the co-pyrolysis of a bituminous

- coal and poplar wood. Chin J Chem Eng. 2022. https://doi.org/10.1016/j.cjche.2022.10.015.
- Lemaire R, Wang W, Menanteau S. Kinetic modeling of the devolatilization of pulverized coal, poplar wood, and their blends in a thermogravimetric analyzer and a flat flame reactor. ACS Omega. 2023;8:29455–67. https://doi.org/10.1021/acsomega.3c03110.
- Doyle CD. Kinetic analysis of thermogravimetric data. J Appl Polym Sci. 1961;5:285–92. https://doi.org/10.1002/app.1961. 070051506.
- Friedman HL. Kinetics of thermal degradation of char-forming plastics from thermogravimetry. Application to a phenolic plastic. J Polym Sci Part C Polym Symp. 1964;6:183–95. https://doi.org/ 10.1002/polc.5070060121
- Cai J, Xu D, Dong Z, Yu X, Yang Y, Banks SW, et al. Processing thermogravimetric analysis data for isoconversional kinetic analysis of lignocellulosic biomass pyrolysis: case study of corn stalk. Renew Sustain Energy Rev. 2018;82:2705–15. https://doi.org/10.1016/j.rser.2017.09.113.
- Açıkalın K. Thermogravimetric analysis of walnut shell as pyrolysis feedstock. J Therm Anal Calorim. 2011;105:145–50. https://doi.org/10.1007/s10973-010-1267-x.
- Lu K-M, Lee W-J, Chen W-H, Lin T-C. Thermogravimetric analysis and kinetics of co-pyrolysis of raw/torrefied wood and coal blends. Appl Energy. 2013;105:57–65. https://doi.org/10.1016/j.apenergy.2012.12.050.
- Song Y, Tahmasebi A, Yu J. Co-pyrolysis of pine sawdust and lignite in a thermogravimetric analyzer and a fixed-bed reactor. Bioresour Technol. 2014;174:204–11. https://doi.org/10.1016/j. biortech.2014.10.027.
- Azizi K, Keshavarz Moraveji M, Abedini Najafabadi H. Characteristics and kinetics study of simultaneous pyrolysis of microalgae *Chlorella vulgaris*, wood and polypropylene through TGA. Bioresour Technol. 2017;243:481–91. https://doi.org/10.1016/j.biortech.2017.06.155.
- Qiu S, Zhang S, Zhou X, Zhang Q, Qiu G, Hu M, et al. Thermal behavior and organic functional structure of poplar-fat coal blends during co-pyrolysis. Renew Energy. 2019;136:308–16. https://doi. org/10.1016/j.renene.2019.01.015.
- Tian H, Jiao H, Cai J, Wang J, Yang Y, Bridgwater AV. Co-pyrolysis of *Miscanthus sacchariflorus* and coals: a systematic study on the synergies in thermal decomposition, kinetics and vapour phase products. Fuel. 2020;262:116603. https://doi.org/10.1016/j.fuel.2019.116603.
- Butler E, Devlin G, Meier D, McDonnell K. Characterisation of spruce, salix, miscanthus and wheat straw for pyrolysis applications. Bioresour Technol. 2013;131:202–9. https://doi.org/10. 1016/j.biortech.2012.12.013.
- Janković B, Manić N, Stojiljković D. The gaseous products characterization of the pyrolysis process of various agricultural residues using TGA–DSC–MS techniques. J Therm Anal Calorim. 2020;139:3091–106. https://doi.org/10.1007/s10973-015-4717-7.
- Pasangulapati V, Ramachandriya KD, Kumar A, Wilkins MR, Jones CL, Huhnke RL. Effects of cellulose, hemicellulose and lignin on thermochemical conversion characteristics of the selected biomass. Bioresour Technol. 2012;114:663–9. https:// doi.org/10.1016/j.biortech.2012.03.036.
- Gao P, Xue L, Lu Q, Dong C. Effects of alkali and alkaline earth metals on N-containing species release during rice straw pyrolysis. Energies. 2015;8:13021–32. https://doi.org/10.3390/en811 12356.
- 53. Xu Q, Ma X, Yu Z, Cai Z. A kinetic study on the effects of alkaline earth and alkali metal compounds for catalytic pyrolysis of microalgae using thermogravimetry. Appl Therm Eng. 2014;73:357–61. https://doi.org/10.1016/j.applthermaleng.2014.07.068.
- Santana JA, Sousa NG, Cardoso CR, Carvalho WS, Ataíde CH.
   Sodium, zinc and magnesium chlorides as additives for soybean



- hulls pyrolysis. J Therm Anal Calorim. 2016;125:471–81. https://doi.org/10.1007/s10973-016-5381-2.
- Liu D, Yu Y, Long Y, Wu H. Effect of MgCl2 loading on the evolution of reaction intermediates during cellulose fast pyrolysis at 325 °C. Proc Combust Inst. 2015;35:2381–8. https://doi.org/10.1016/j.proci.2014.05.026.
- Zhu C, Maduskar S, Paulson A, Dauenhauer P. Alkaline-Earth-Metal-Catalyzed Thin-Film Pyrolysis of Cellulose. Chem-CatChem. 2016. https://doi.org/10.1002/cctc.201501235.
- 57. Hu S, Jiang L, Wang Y, Su S, Sun L, Xu B, et al. Effects of inherent alkali and alkaline earth metallic species on biomass pyrolysis at different temperatures. Bioresour Technol. 2015;192:23–30. https://doi.org/10.1016/j.biortech.2015.05.042.
- 58. Dalluge DL, Kim KH, Brown RC. The influence of alkali and alkaline earth metals on char and volatile aromatics from fast pyrolysis of lignin. J Anal Appl Pyrolysis. 2017;127:385–93. https://doi.org/10.1016/j.jaap.2017.07.011.
- Arora JS, Chew JW, Mushrif SH. Influence of alkali and alkaline-earth metals on the cleavage of glycosidic bond in biomass pyrolysis: a DFT study using cellobiose as a model compound. J Phys Chem A. 2018;122:7646–58. https://doi.org/10.1021/acs.jpca.8b06083.
- Fischer O, Lemaire R. Thermogravimetric analysis and kinetic modeling of the AAEM-catalyzed pyrolysis of spruce wood,

- wheat straw, switchgrass, miscanthus and swine manure. Proceedings of the combustion institute Canadian section (CI/CS), Spring Technical Meeting 2024.
- 61. Bernades GP, de Pra AM, Poletto M. Effect of alkaline treatment on the thermal stability, degradation kinetics, and thermodynamic parameters of pineapple crown fibres. J Mater Res Technol. 2022;23:64–76. https://doi.org/10.1016/j.jmrt.2022.12.179.
- Ellison C, Garcia-Perez M, Mullen CA, Yadav MP. Thermochemical behavior of alkali pretreated biomass a thermogravimetric and Py-GC/FID study. Sustain Energy Fuels. 2023;7:3306. https://doi.org/10.1039/D3SE00213F.
- Saddawi A, Jones JM, Williams A. Influence of alkali metals on the kinetics of the thermal decomposition of biomass. Fuel Process Technol. 2012;104:189–97. https://doi.org/10.1016/j.fuproc. 2012.05.014.

**Publisher's Note** Springer Nature remains neutral with regard to jurisdictional claims in published maps and institutional affiliations.

